DEMOCRATIC AND POPULAR REPUBLIC OF ALGERIA

MINISTRY OF HIGHER EDUCATION AND SCIENTIFIC RESEARCH
UNIVERSITY MOHAMED BOUDIAF OF M'SILA - M'SILA

Faculty of Sciences

Department of Physics

Enrolment N°:PH/ENR/20/2025

DOMAINE: SCIENCE OF MATTER

FIELD : PHYSICS

OPTION : ENERGY PHYSICS AND RENEWABLE ENERGY

Memory Submitted for Obtaining Diploma of Academic Master

Presented By:

Morzouglal Ahmed

Entitled

Effect of thickness on properties of Mn-doped ZnO thin films for solar cell application

Defended on: 23 / 06 / 2025

In front of the jury composed of:

Dr. Kherifi Djelel	**University of M'sila**	**Chairman**
Dr. Benrezgua Elhadj	**University of M'sila**	**Supervisor**
Pr. Deghfel Bahri	**University of M'sila**	**Co-Supervisor**
Dr. Amari Rabie	**University of M'sila**	**Examiner**
Dr. Boukhari Amar	**University of M'sila**	**Examiner**

Academic year: **2024 /2025**

ACKNOWLEDGEMENTS

Praise be to **Allah** for the success in the realization and completion of this work.

I would like to express my sincer e gratitude to my supervisor **Dr. BENREZGUA Elhadj**, I am grateful to him for having directed my work while leaving me free to explore my ideas. I thank him for his advice, opinion, help, and for being present and motivating.

I would also like to warmly thank my co-supervisor **Pr. DEGHFEL Bahri** for his valuable assistance, guidance, and encouragement, which contributed greatly to the progress and completion of this work.

It is an honour for me that **Dr. KHERIF Djelel** has accepted to chair the jury.

My sincere thanks go to **Dr. AMARI Rabie** and **Dr.Boukhari Amar** for accepting to participate as examiners in this jury.

My heartfelt thanks go to my dear father for his patience and constant support, to my siblings, my friends, and everyone who stood by me and contributed to this work. I cannot fail to mention my late mother "may Allah have mercy on her" whose prayers and love continue to guide me every step of the way. This project would not have been possible without the collective support of all these wonderful people.

Finally, I would like to express my deepest thanks to all the academic and administrative staff of the Physics department at MOHAMED Boudiaf University - M'sila.

.

M. Ahmed 2025

TABLE OF CONTENTS

CHAPTER III: Results and discussions

General introduction

Considerable efforts are recently focused on semiconducting metal oxides materials such as TiO_2, SnO_2, ZnO and CuO, which have been the subject of a great deal of many researches and have aroused great interest in the academic and industrial world. At the nanoscale form, these materials offer a remarkable improvement in their properties compared to the corresponding micro-and macro-materials. The development of these materials is related to their attractive physical properties and advantages compared to other materials (stable, non-toxic, low cost, etc). These materials (oxides) are good candidates for applications in different technological sectors, especially in photovoltaics and optoelectronics**[1]**.

Zinc oxide belongs to the II-VI semiconductor group, featuring a direct band gap of 3.37 eV and an exciton binding energy of 60 meV at ambient temperature. These properties, combined with its high chemical stability, non-toxicity, low growth temperature, and transparency in the visible spectrum, position ZnO as a promising material for various applications. ZnO has potential uses in devices such as transparent electrodes **[2]**, gas sensors **[3]**, solar cells **[4]**, spintronic devices **[5]**, and UV light-emitting diodes (LEDs) **[6]**. Numerous methods for fabricating ZnO thin films have been explored, including pulsed laser deposition **[7]**, RF magnetron sputtering **[8]**, molecular beam epitaxy (MBE) **[9]**, spray pyrolysis **[10]**, and chemical vapor deposition **[11]**. The sol-gel method, in particular, has gained interest for its simplicity, cost-effectiveness **[12, 13]**, and benefits like large-area deposition and uniform film thickness **[14]**. The impact of film thickness on ZnO's properties has been thoroughly investigated using various physical and chemical synthesis methods, further expanding its potential for a wide range of device applications. **[15-19]**.

In recent years, numerous studies have focused on improving the properties of ZnO by doping it with elements such as Co, Mn, Al, and Mg. **[14]**. Manganese (Mn) has been extensively studied as a dopant, particularly in Mn-doped ZnO (MZO) thin films, where various physical properties have been explored under different experimental conditions **[20]**. This research is driven by the potential of ZnO for optoelectronic applications in the blue and ultraviolet spectral ranges **[21]**, as well as its unique characteristics as a dilute magnetic semiconductor, including room temperature ferromagnetism and semiconductivity. Notably, the properties of MZO thin films are strongly influenced by film thickness. Research on films deposited through RF magnetron sputtering indicates that increasing the thickness improves crystallinity and grain size, while decreasing strain, average transmittance, and band gap energy. These films generally crystallize in the wurtzite structure, exhibiting a preferred orientation along the (002) c-axis.**[22-24]**.

The first chapter presents a experimental literature review. This review aims to provide a timely overview on the development of MZO thin films by sol-gel, spin- and dip-coating as reported in literature survey from 2010 to 2024. Starting with preparation materials, solution preparation, depositing the materials and finally the properties of thin films. Properties of thin films such as structural, morphologies and, optical, bonding, properties.

The second chapter presents a general description of the sol-gel process, describes the experimental spin coating technique used to prepare thin films, discuss the protocol for the elaboration of Mn doped ZnO in thin films. The morphological, structural and optical characterization techniques will be briefly explained.

The third chapter is dedicated to presenting and discussing the obtained results and is divided into two parts. The first part focuses on the fabrication of 7% manganese-doped zinc oxide (MZO) thin films with varying number of layers (1 layer, 2 layers, and 4 layers), synthesized using the spin coating method. The structural, morphological, and optical properties of the MZO thin films are then characterized through various techniques.

Finally, a summary of the main conclusions drawn from the different characterizations of the MZO thin films is presented.

References

[1] S.-H. Jeong, J.-H. Park, and B.-T. Lee, "Effects of Mg doping rate on physical properties of Mg and Al co-doped Zn1− x− 0.02 MgxAl0. 02O transparent conducting oxide films prepared by rf magnetron sputtering," *Journal of alloys and compounds,* vol. 617, pp. 180-184, 2014.

[2] H.-C. You, Y.-W. Tu, Y.-H. Lin, and S.-H. Shieh, "The transistor characteristics of zinc oxide active layer with different thickness of zinc oxide thin-film," in *2012 International Symposium on Computer, Consumer and Control*, 2012: IEEE, pp. 858-861.

[3] L. Zhu and W. Zeng, "Room-temperature gas sensing of ZnO-based gas sensor: A review," *J Sensors Actuators A: Physical,* vol. 267, pp. 242-261, 2017.

[4] M. Giannouli and F. Spiliopoulou, "Effects of the morphology of nanostructured ZnO films on the efficiency of dye-sensitized solar cells," *Renewable Energy,* vol. 41, pp. 115-122, 2012.

[5] N. Rajamanickam, S. Rajashabala, and K. Ramachandran, "Effect of Mn-doping on the structural, morphological and optical properties of ZnO nanorods," *Superlattices and Microstructures,* vol. 65, pp. 240-247, 2014.

[6] S. Pearton and F. Ren, "Advances in ZnO-based materials for light emitting diodes," *Current Opinion in Chemical Engineering,* vol. 3, pp. 51-55, 2014.

[7] A. Smaali *et al.*, "Pulsed laser deposited transparent and conductive V-doped ZnO thin films," *J Thin Solid Films,* vol. 700, p. 137892, 2020.

[8] Y. Bouznit, Y. Beggah, and K. Djessas, "RF magnetron sputtering of ZnO and Al-doped ZnO films from ceramic and nanopowder targets: a comparative study," *Journal of sol-gel science and technology,* vol. 61, pp. 449-454, 2012.

[9] H. Kato, M. Sano, K. Miyamoto, and T. Yao, "Homoepitaxial growth of high-quality Zn-polar ZnO films by plasma-assisted molecular beam epitaxy," *Japanese journal of applied physics,* vol. 42, no. 8B, p. L1002, 2003.

[10] R. S. Gaikwad, S. B. Jagdale, P. B. Pol, K. C. Mohite, and B. N. Pawar, "Effect of concentration of precursor on intrinsic ZnO thin films by spray pyrolysis," *Asian Journal of Multidisciplinary Studies,* vol. 2, no. 5, p. 110, 2014.

[11] R. Müller *et al.*, "Chemical vapor deposition growth of zinc oxide on sapphire with methane: initial crystal formation process," *J Crystal Growth and Design,* vol. 19, no. 9, pp. 4964-4969, 2019.

[12] F. Baig and G. S. Butt, "Impact of copper doping on optical, UV induced wettability and photo-catalytic properties of sol-gel synthesized ZnO thin films," *J Optik,* vol. 288, p. 171196, 2023.

[13] I. Y. Bouderbala, A. Guessoum, S. Rabhi, O. Bouhlassa, and I.-E. Bouras, "Optical band-diagram, Urbach energy tails associated with photoluminescence emission in defected ZnO thin films deposited by sol–gel process dip-coating: effect of precursor concentration," *Applied Physics A,* vol. 130, no. 3, p. 205, 2024.

[14] W. Chen, J. Wang, and M.-r. Wang, "Influence of doping concentration on the properties of ZnO: Mn thin films by sol–gel method," *Vacuum,* vol. 81, no. 7, pp. 894-898, 2007.

[15] D. Pal *et al.*, "Effect of substrates and thickness on optical properties in atomic layer deposition grown ZnO thin films," *Applied surface science,* vol. 421, pp. 341-348, 2017.

[16] A. Namoune, T. Touam, and A. Chelouche, "Thickness, annealing and substrate effects on structural, morphological, optical and waveguiding properties of RF sputtered ZnO thin films," *Journal of Materials Science: Materials in Electronics,* vol. 28, pp. 12207-12219, 2017.

[17] V. Kumar, S. K. Singh, H. Sharma, S. Kumar, M. Banerjee, and A. Vij, "Investigation of structural and optical properties of ZnO thin films of different thickness grown by pulsed laser deposition method," *Physica B: Condensed Matter,* vol. 552, pp. 221-226, 2019.

[18] A. Mortezaali, O. Taheri, and Z. Hosseini, "Thickness effect of nanostructured ZnO thin films prepared by spray method on structural, morphological and optical properties," *Microelectronic Engineering,* vol. 151, pp. 19-23, 2016.

[19] N. Kakati, S. H. Jee, S. H. Kim, J. Y. Oh, and Y. S. Yoon, "Thickness dependency of sol-gel derived ZnO thin films on gas sensing behaviors," *Thin Solid Films,* vol. 519, no. 1, pp. 494-498, 2010.

[20] M. Xin, L. Z. Hu, D.-P. Liu, and N.-S. Yu, "Effect of Mn doping on the optical, structural and photoluminescence properties of nanostructured ZnO thin film synthesized by sol–gel technique," *Superlattices and Microstructures,* vol. 74, pp. 234-241, 2014.

[21] S. T. Shishiyanu, T. S. Shishiyanu, and O. I. Lupan, "Sensing characteristics of tin-doped ZnO thin films as NO2 gas sensor," *Sensors and Actuators B: Chemical,* vol. 107, no. 1, pp. 379-386, 2005.

[22] Z. N. Kayani, F. Nazir, S. Riaz, and S. Naseem, "Structural, optical and magnetic properties of manganese zinc oxide thin films prepared by sol–gel dip coating method," *Superlattices and microstructures,* vol. 82, pp. 472-482, 2015.

[23] R. Rajalakshmi and S. Angappane, "Effect of thickness on the structural and optical properties of sputtered ZnO and ZnO: Mn thin films," *Journal of alloys and compounds,* vol. 615, pp. 355-362, 2014.

[24] M. Venkaiah and R. Singh, "Effect of thickness on structural, optical and mechanical properties of Mn doped ZnO nanocrystalline thin films RF sputtered in nitrogen gas environment," *Superlattices and Microstructures,* vol. 72, pp. 164-171, 2014.

CHAPTER I

Literature review

I. 1. A review on synthesis and properties of manganese doped zinc oxide thin films

I.1.1. Introduction

Hexagonal Zinc oxide (ZnO) with wurtzite structure and tetrahedrally coordinated atoms, is the most stable phase; which usually exhibits a preferred orientation along *c*-axis, a spontaneous polarization **[1]** and a mix of ionic and covalent type Zn-O bonding **[2, 3]**. At ambient experimental conditions, transparent ZnO having a high exciton binding energy (60 meV) and direct large band-gap (Eg) (3.37 eV), is a promising candidate for several applications such as gas sensor **[4, 5],** photo catalytic processes **[6, 7]**, transparent conducting electrodes **[8, 9]**, laser system **[9, 10]**, light emitting diode **[11, 12]**.

Fabrication of transparent conducting oxides (TCO) thin films with desired properties, like grain shape and size, surface morphology, band gap, transmittance, growth mode, is important task for different practical applications. Preparation conditions, synthesis method and doping process are the main factors for controlling such properties. Nontoxic and chemically stable TCO such as ZnO, have several interesting properties and they have been widely doped with transition metal elements such as manganese (Mn). In addition to these advantages, the elaboration of TCO by a low cost and simple method, like sol-gel process, constitute a combination that attract the attention of several researchers to exploring the effect of the preparation conditions on the properties of Mn doped ZnO (MZO) thin films. There are many factors influencing the growth mode of MZO thin films and then their properties **[13-20]**. These factors are subdivided into three main categories, i.e., dopant element, synthesis method and appropriate environment. Reproducibility with desired properties remains to be a major problem in thin films preparation and this must be resolved before they can be used in various opto-electronics applications. Numerous techniques have been used to improve the properties of ZnO films such as spray pyrolysis **[13]**, pulsed laser deposition (PLD) **[14]**, reactive magnetron sputtering **[15]**, molecular beam epitaxy **[16],** chemical vapor deposition (CVD) **[17]**, dip coating **[20] and** spin coating **[18, 19]**.

ZnO from sol-gel solution, used as source for spin coating or dip coating, is a relatively low cost and simple process. It possesses the ability to achieve uniform MZO nanostructures at low temperatures and under very controlled and stable conditions. Transition metals doped ZnO thin films have been studied with various elements such as Silver **[11],** manganese (Mn)**[21],** Aluminium **[8]**, Antimony (Sb) **[14]**, Cobalt (Co) **[18]** and Sodium (Na) **[20]**. Among them, Mn is extensively used to enhance the properties of ZnO host lattice such as transparency,

ferromagnetism, crystalline quality and conductivity**[22, 23].** manganese (Mn) is a suitable one for the incorporation into the ZnO lattice due to its high solubility with respect to ZnO**[24]**.

Since ZnO is quite common materials for different applications, many reviews on ZnO were published for the last 10 years. However, on 'doped' and 'thin film' of ZnO are still limited. For example, Fan et al **[25]** considered the copper as p-type ZnO promising materials in addition to elements from different group and they focused only on the application of such materials; Zhu et al. **[26]** also pointed out the copper as a potential candidate, among others, to the room-temperature gas sensing of ZnO-based gas sensor; later on, B. L. Martínez-Vargas et al. **[27]**explained Explained the different synthesis techniques of the ZnO-MnO nanocomposite and highlighted their impact on the structural and surface morphologies of the prepared materials; recently, A. Boukhari et al **[28]**investigated the effect of thickness on the structural, morphological, electronic, and optical properties of pure and 7% Mn-doped ZnO thin films prepared by the sol–gel spin coating method, employing both experimental techniques and DFT+U calculations to examine the influence of film thickness and Mn incorporation on the physical properties and electronic structure of ZnO-based materials.

To the best of our knowledge, reviews on specifically Mn dopant ZnO thin films, have not been reported yet. Its interesting to have a review devoted mainly to the properties of ZnO thin films based on the doping with a specified element, i.e., Mn and prepared by a simple and low-cost method, i.e. sol-gel. The compilation of articles will be providing a huge database to the researchers working on MZO thin films properties.

This review aims to provide a timely overview on the development of Mn thin films by sol-gel, spin- and dip-coating as reported in literature survey from 2010 to 2020. Starting with preparation materials, solution preparation, depositing the materials and finally the properties of thin films. Properties of thin films such as structural, morphologies, electronic, optical, bonding, vibrational and magnetic properties as well as chemical composition, will be reviewed in detail.

I.1.2. Synthesis of MZO thin films

The preparation and growth technique of raw materials played an important role in controlling the properties of thin films. Different physical and chemical properties can be found for the same deposited material by various elaboration techniques, in which its properties are strongly influenced by the experimental conditions. Sol-gel process is a low cost and simple

chemical synthesis methods of MZO thin films. It is also involving several parameters such as additive, solvent, substrate, solution stirring and aging time, preheating, coating method, and annealing**.** The sol–gel process or soft chemistry, which consists of preparing a sol, its gelation, and solvent removal is well suited for the synthesis of composite nanopowders, oxide nanoparticles, and organic–inorganic materials using spin or dip routes. The key advantages of this process is the ability to achieve uniform nanostructures at low temperatures, while the introduction of impurities from byproducts of the reaction is considered its major disadvantage **[29]**.

Focussing on findings from various sources**[30-36],** parameters involved in the sol-gel process during elaboration of MZO thin films, such as source of the precursor and its concentration, type of solvent, additive species and their concentration, stirring and aging time of the sol, preheating, annealing, coating method, speed and type of the substrate, will be discussed in detail in the following section;

i. Precursors: the viscosity of the sol-gel is controlled by changing the concentration of the precursors, which influences the MZO film thickness,

ii. Solvents: the choice of solvent is important for MZO thin films preparation in such that precursors are soluble in the solvent medium and get easily decomposed into volatile compounds

iii. Additives: structural properties and growth mode of MZO thin films are found to be based on the concentration of additives,

iv. Substrate: morphology and growth mode of MZO films are influenced by the deposition on different kinds of substrates,

v. Heating and annealing coating: the amount of porosity can be lowered by increasing the annealing temperature, which influences the surface area of the MZO thin film,

vi. Speed and coating mode: higher angular velocities lead to thin and uniform layers on flat substrates, whereas in dip coating process, higher withdrawal speeds result in thicker films.

The sol-gel is dropped onto a substrate, which rotates at high speed in the spin coating method. This causes the excess liquid to flow out of the substrate (**Figure 1a**). The constant speed rotation allows to cover the substrate with uniform decreasing of the film thickness. Evaporation then removes the solvent leaving behind a dry solid film **[37]**. Finally, the nanoparticles aggregate to agglomerates by drying and heating **[38, 39]**. In the dip-coating method, a substrate is immersed into a solution containing the sol-gel and then removed at a specific speed under very controlled and stable conditions to obtain a regular porous film (**Figure 1b**). Films deposited by these technique are usually X-ray amorphous and require a

calcination step to obtain crystallization **[37, 40].** There are many works published on synthesis of MZO thin films by different routes, elaborated either by spin-coating **[41-43]** or dip-coating**[44, 45].**

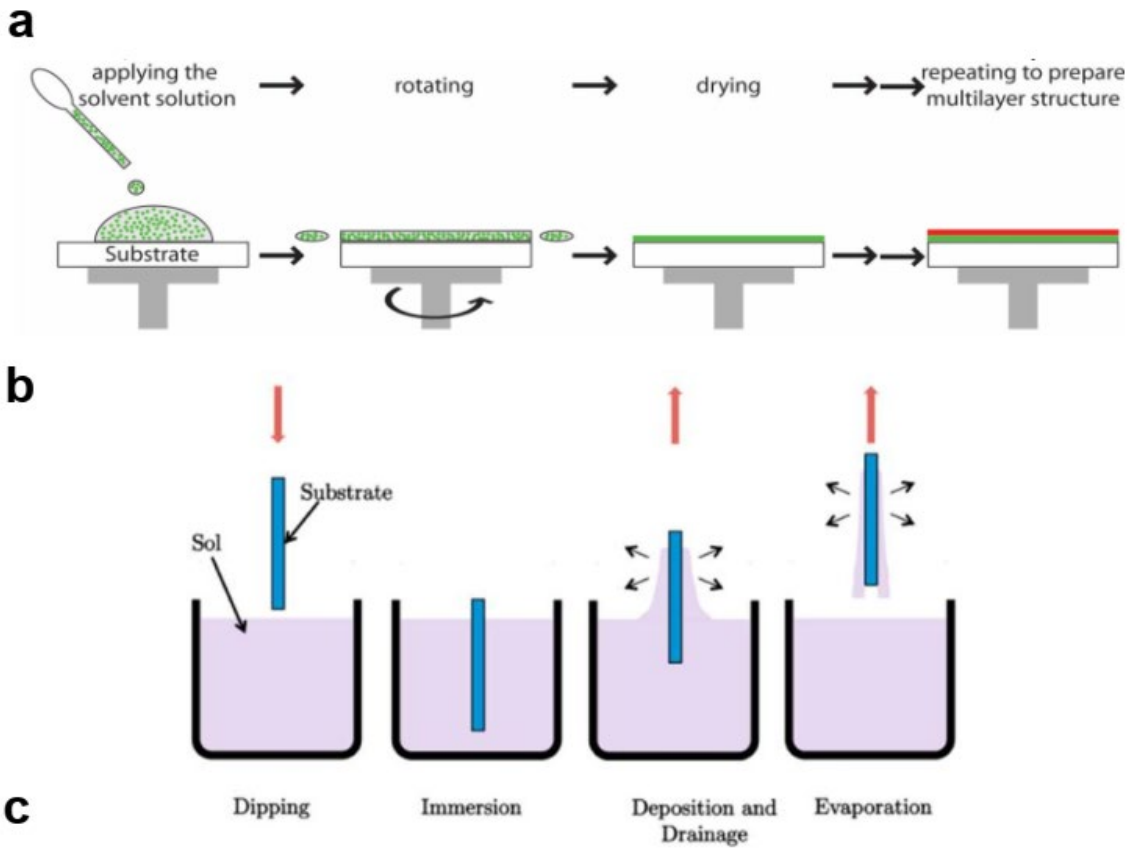

Figure I.1. Schematic diagram of **(a)** sol gel process by spin-coating route, reprinted from Ref. **[46]**, **(b)** dip-coating route, reprinted from Ref. **[47]**.

The mixing of reagents and precursors leads to the formation of a sol by either hydrolysis or polymerization reactions. The adding of polymers converts the sol to gel after thermal treatments**.** The gel can be deposited onto substrates and calcined to obtain the final material as thin films of different form such as nanospheres, nanorods, nanoflakes, nanotubes, nanoribbons, nanospheres and nanofibers. The following section summarizes the various precursors, solvents and additives used in the preparation of MZO thin films and deposited onto substrates by sol-gel method **[48]:**

i. ***Zinc and manganese precursors*****:**

Zinc acetate dehydrate (ZAD; $Zn(CH_3COO)_2 \cdot 2H_2O$) is the most often used zinc precursors **[49-60]** and, less favorable, the zinc acetate anhydrous (ZA; Zn $(CH3COO)_2$) **[61, 62]** for ZnO thin films elaboration. For Mn dopant, several manganese precursors have been additionally used for MZO thin films elaboration such as manganese acetate (MA; Mn $(CH3COO)_2$)**[63]**, manganese nitrate (MN; $Mn(NO_3)_2$), manganese nitrate tetrahydrate (MNT; $(MnNO_3)_2$ $3H_2O$) **[64],** manganese sulfate monohydrate (MSM; $MnSO_4 \cdot H_2O$)**[65]**, manganese acetate dihydrate (MAD; Mn $(CH3COO)_2 \cdot$ 2H2O) manganese acetate tetrahydrate (MAT; Mn (CH3COO)2·2H2O)**[66]**, manganese nitrate hexahydrate (MNH; $MnH_{12}N_2O_{12}$)**[67]** and manganese chloride(MC; $MnCl_2$)**[68]**.

ii. ***Solvents***

Different types of alcohols which are used as solvents, i.e. ethanol (EtOH; C_2H_5OH), methanol (MeOH; CH_3OH), isopropanol [IPA; C H 3 CH(OH)-CH_3], 2-methoxyethanol [2-ME; $CH_3O(CH_2)_2OH$] and 2-propanol [2-PrOH; IPA; $(CH_3)_2CHOH$]. Ethanol and 2-methoxyethanol the are the most used solvents**[67, 69-72]**.

iii. ***Additives*****:**

To facilitate the complete dissolution precursors-alcoholic media and the formation of a stable sol, additives are used **[73]**. In addition to the most often used, i.e. monoethanolamine [MEA; $(HOCH_2CH_2)NH_2$], there are other additives used in the MZO thin films elaboration, namely, diethanolamine [DEA; $(HOCH_2CH_2)_2NH$], triethanolamine [TEA; $(HOCH_2CH_2)_3N$], acetic Acid (Ac. Ac.; CH_3COOH) and lactic Acid (Lactic Ac.; $CH_3CHOHCOOH$) **[70, 74-76]**. Sometimes, it is preferable to use an additive instead of other in certain circumstance for better dissolution of the mixture. Moreover, most of the studies on MZO thin films are restricted to low Mn doping concentrations. This might be attributed to the limited solubility of Mn in ZnO host lattice or the appearance of other phase like MnO, MnO_2 or Mn_2O_3 lattices**[23] [77]**.

iv. *Substrate*:

Preparation of MZO thin film by sol-ge are mostly deposited on glass substrate**[21, 78-80]**. Later, the heat treatment (below 100 °C) on sample still producing clear and homogenous solution**[81]**. Two mechanisms due the nucleation at the film/substrate interface, were proposed for the orientation of the films on the glass substrates. The first is favored on smooth surfaces with the tendency of nuclei to develop a minimum free energy configuration. The second results from survival of nuclei having

an energetically unstable plane parallel to the substrate **[16].** Spin and dip coating methods also enables MZO thin film deposition on a variety of specific types of substrate including quartz**[82]**, silicon **[78]** soda lime**[83]**, ITO**[84]** and borosilicate**[85]**.

v. *Heat treatment*:

The synthesis of MZO thin film needs two heat treatment normally applied for; pre-heat treatment which removes the solvent leaving behind a dry solid film, and annealing by which nanoparticles aggregate to agglomerates. Pre-heat treatment depends on additives and solvent, but it should be higher than the boiling point of them **[86]**. Some additives-solvent combinations, like monoethanolamine and 2-methoxyethanol (MEA-2-ME), need a higher temperature (~250-500 °C) while a low temperature (~70-150 °C) is sufficient for some other combinations, like diethanolamine-2-propanol (DEA-2-PrOH), during evaporation and removal of the organic compounds, to grow (002) oriented films. The annealing temperature, which generally varies within a range of 400-800 °C, is an important factor governing the orientation of the crystallites and the well-crystallization of the films[86]. The formation of MnO phase is possibly observed if the temperature acceding 800 °C, **[77].**

I.1.3. Structural properties of MZO thin films

Structural analysis by X-ray diffraction (XRD) is an analytical technique primarily used for providing information on the structure and phase of a crystal and can also confirm the incorporation of defects in each host lattice. Various parameters within the crystal such as the lattice parameters, crystallite size and number of phases, stress and strain, which were deduced from the diffraction peaks of XRD analysis, are then presented and discussed in this section. Manganese (Mn), a group VIIB element, typically exhibits valence states of +2 or +3, depending on its chemical structure and bonding environment. Thus, manganous oxide (MnO),

manganese dioxide (MnO_2), and manganese(III) oxide (Mn_2O_3) are the three stable types of manganese oxide. The radii of Mn^{2+} (81 pm) and Mn^{3+} (65 pm) ions are similar to that of Zn^{2+} ion (83 pm), which makes Mn a potential doping candidate for ZnO**[87]**.

XRD techniques are powerful, non-destructive tool for material characterization. It provides the first information about the structural properties of the materials, before any other characterization can be done. For thin films deposited on to the substrate, the X-ray beam enters with a small angle of incidence (0.5–2), known as grazing incidence X-ray diffraction GIXRD (**Figure I.2**) **[88]**, which has been used to characterize MZO thin films**[33, 89]**. In this case, the incidence angle is fixed, and the crystallites are randomly oriented which limits the X-ray penetration into the thin films. One of the most critical conditions for XRD analysis of samples is proper sample preparation. Since peak broadening is negligible for larger particles, XRD is generally useful for nanoscale crystallites with diameters below 100–200 nm. For very small particles with a diameter below 2–3 nm, the peak width cannot be reliably measured or even observed. Furthermore, since the Scherrer equation ignores internal particle strain and defects, which can cause peak broadening, the particle size determined by XRD should not be regarded as absolute measure of crystallite size **[90].**

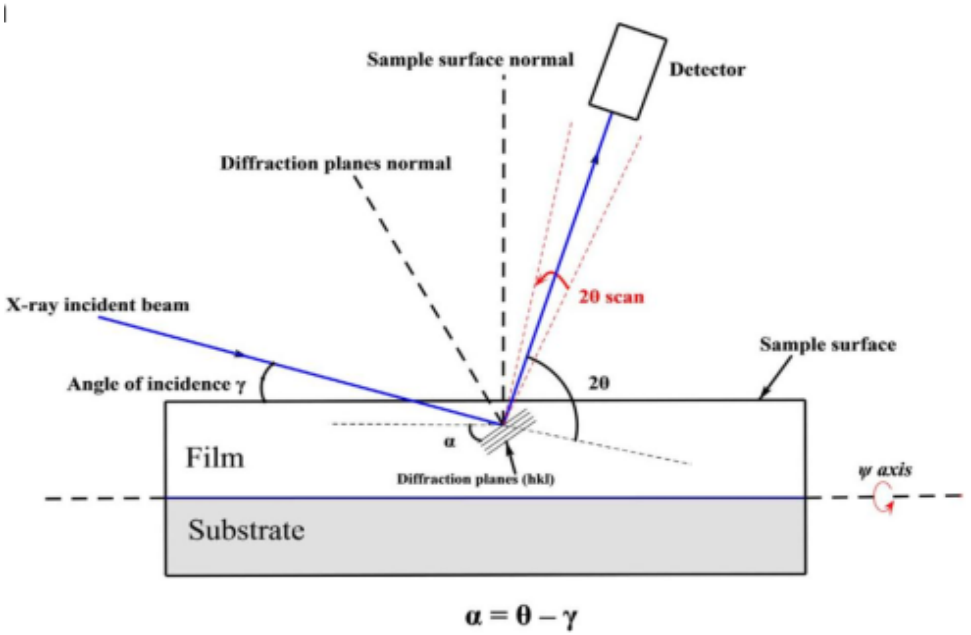

Figure I.2. Schematic diagram of grazing incidence X-ray diffractometry **[88].**

XRD spectra of pure ZnO thin films generally shows a peak at the Bragg angle of ~34.5°, which is assigned to (002) plane **[91, 92]**. Moreover, (100) peak at ~31.9° and (101) peak at ~36.4° can also be observed in some cases **[53, 93]**.

The incorporation of Mn at low concentrations into the ZnO host lattice does not exhibit any additional secondary phases (such as MnO or MnO_2) and preserves the wurtzite crystal structure of ZnO. This is attributed to the substitutional incorporation of Mn^{2+} ions into the ZnO lattice, facilitated by the similarity in ionic radii between Mn^{2+} (0.66 Å) and Zn^{2+} (0.74 Å)**[94]**. Under such conditions, Mn-doped ZnO (MZO) prefers the (002) plane as the dominant orientation among several possible planes corresponding to (100), (002), (101), (102), (110), (103), (112) and (004) peaks of ZnO observed in the XRD patterns ($P6_3mc$ space group; JCPDS card No. 00-36-1451)**[94]**. This asserts that MZO thin films possess a polycrystalline nature. However, The other Mn_3O_4 phase can appear by increasing content of Mn dopant, 10 mol.%**[94]**, with emerging a (121) new peak. The intensity of (002) peak is generally increased, especially at high Mn concentration, leading to the degradation of the (002) preferential orientation of MZO thin films with the enhancement of other orientations like (100) and (101)**[94]**. This was affected to heterogeneous nucleation proces**[95]**.

The variation occurred in intensity and position of different peaks of XRD pattern by Mn doping were presented in the literature as a function of diffraction angle for ZnO and MZO samples **[96, 97]**. A slight shift in the peak position towards lower diffraction angles is obtained with the increase of Mn concentration. The observed shift is attributed to the substitution of Mn atom at Zn atom site where the ionic size of Mn^{2+} is slightly smaller than Zn^{2+},This can also explain the change occurred in other related parameters, such as lattice constants, crystallite size and strain and stres **[98]**. On the other hand, the diffraction peaks of XRD analysis can give other information within crystal such as the lattice parameters, crystallite size and number of phases, and that is through famous formulas and appearing and/or disappearing of some peaks in the XRD pattern of MZO thin films**[98]**.

The increasing level of Mn content can influence the lattice strain**[70, 82]**. The strain variation is explained by the presence of excess Mn dopant at grain boundarie**[83]**. It is also ascribed to the intrinsic stress due to the impurities and defects in the host lattice**[70]**.

The lattice constants $a = b$ and c can be usually calculated from XRD patterns for pure and MZO thin films**.** It is observed that lattice constants are slightly affected by Mn content. This is mainly due to the strain induced by the incorporation of Mn into ZnO host lattice, which

leads to the change in bond angle along *c* axis between Zn-O planes (120° for hexagonal wurtzite ZnO) where the ionic radius of Mn^{2+} (0.66A˚) is slightly smaller than that of Zn^{2+} (0.74A˚)**[98]**.

It is also found that the increasing of Mn doping influences the crystallite size (D). The crystallite size presents an decrease with increasing Mn content, especially at higher thickness**[82]**, while an decrease followed by a increase is marked at lower thickness**[78]**. However, a decrease in the crystallite size value is also noticed in the literature**[21, 83]**.

In addition, the preferential orientation and its intensity of MZO films for a given concentration depend on the deposition method **[86, 99]**. Moreover, the increasing level of Mn concentration plays an important role in the change of the preferential orientation from one direction to another, where the growth mode of grains translates from c-axis growth perpendicular to the substrate to lateral one**[68]**.

The thicknesses of MZO thin films, elaborated by different methods at various experimental conditions were measured by different techniques such as cross sectional SEM 2D-image, Profilometer, envelope method based on transmittance measurement. The compiled data exhibit both an increase **[100]** and a decrease**[82]** in the thickness with increasing Mn content. This may be attributted to the growth mode of grains, perpendicular or lateral, which is affected by Mn incorporation as well as the experimental conditions such as substrate type and deposition mode. However, slight variation of thickness is also noticed in the literature, especially at lower Mn concentrations**[70]**.

The shift of the main peaks position and their intensity from the XRD analysis of MZO thin films were intensively investigated for lower and somewhat higher concentrations**[87, 101]**. Most of reports exhibited a shift of main peak (002) position towards higher diffraction angle (2θ) with the increase of Mn doping concentration **[28, 102]**. This behaviour was explained by taking into account that the ZnO host lattice might be doped by Mn^{2+} ions, whose ionic radius (0.66 Å) is slightly smaller than that of Zn^{2+} (0.74 Å), which were identified experimentally in the ZnO by XPS spectroscopy**[78]**.

Summary of the main findings of the gathered results from previously cited works, can then be drown as follow,

i. At lower Mn doping levels, Mn^{2+} ions are substitutionally incorporated into the ZnO lattice without the formation of secondary phases. This is facilitated by the close similarity in ionic radii between Mn^{2+} (0.66 Å) and Zn^{2+} (0.74 Å), leading to the conservation of the hexagonal wurtzite structure and the dominance of the (002) preferential orientation.

ii. An increase in Mn concentration induces a transformation in the grain growth mode from a c-axis oriented growth (perpendicular to the substrate) to lateral growth. This transition affects the film morphology, thickness, and preferred orientation, depending on deposition conditions.

iii. At elevated Mn doping levels , secondary manganese oxide phases such as Mn_3O_4 may appear, as evidenced by the emergence of new diffraction peaks (e.g., (121)) and a reduction in the intensity of the (002) peak. This behavior is associated with the saturation of Mn solubility in the ZnO lattice and enhanced heterogeneous nucleation.

iv. XRD patterns exhibit a shift in the position of main diffraction peaks, particularly the (002) peak, with increasing Mn content. A shift towards lower angles is often reported and attributed to the incorporation of Mn^{2+} into Zn sites, causing slight lattice distortions due to ionic size mismatch.

v. Mn doping introduces lattice strain and intrinsic stress due to the presence of dopants and structural defects. These factors lead to changes in lattice parameters (especially along the c-axis), as well as a general reduction in crystallite size with increasing Mn content, particularly in thicker films. In some cases, a non-monotonic trend in crystallite size is observed depending on film thickness and deposition conditions.

I.1.4. Morphological properties of MZO thin films

To investigate the smallest of internal thin films, results issued from Atomic Force Microscopy (AFM) and Scanning Electron Microscopy (SEM) are investigated in this. So, the micrographs give further confirmation to results issued from XRD patterns due to ability to reveal the grain size and the surface roughness of MZO thin films. In the tow following sections, we will summarize the various factors related to preparation method and adding materials that influencing the morphological parameters of MZO thin films such as particles agglomeration, grain size and shape, growth mode and roughness.

I.1.4.1. AFM morphology of the MZO thin films

Atomic Force Microscopy (AFM) is based on measuring the forces between a given sample surface and a sharp tip which moves across it and generates three or two dimensional topographic map of the surface (**Figure I.3**) **[103].** Depending on the cantilever oscillation, the AFM can be operated in three common modes: contact, non-contact, and tapping. For soft samples, non-contact mode is preferable over contact mode, in which the AFM measurement does not suffer from tip or sample degradation effects. AFM does not request any special treatment during MZO sample preparation such as its coating with a conducting film and vacuum **[104]**.

AFM analysis have been reported in the literature on MZO thin films at various Mn doping levels expressed as atomic percent (limited to low x **[82, 105]** and extended to higher *x* **[106]),** weight percent **[107]** or molar percent**[68]**. Then, two and three-dimensional AFM images **[37, 108]**as well as morphological parameters, such roughness and grain size, are usually extracted from the AFM analysis of the samples. A nanofiber-like morphology was observed for lower Mn-doped ZnO films **[42]**, which differs from the mixed granular and columnar microstructure reported in other studies at higer Mn doping concentrations. Pure and MZO thin films with Mn concentration of 1, 3 and 5 mol%, exhibited a closely packed and granular features for undoped films and larger grains densely packed for Mn doped films**[109]**. Other surface morphologies from previous works are also tabulated in sake of comparison and to give more insights on the influence of various preparation parameters on surface morphology. Some works noticed the decrease in the surface roughness with increasing Mn content **[68]** while some others marked its increase at lower *x* followed by a decrease at lower *x* **[108]**. However, a increase in the surface roughness is also marked in the literature**[77]**. Therefore, it

has been demonstrated that the particle shape and size as well as surface morphology were strongly dependent on the synthesis condition as well as on the range of Mn concentration.

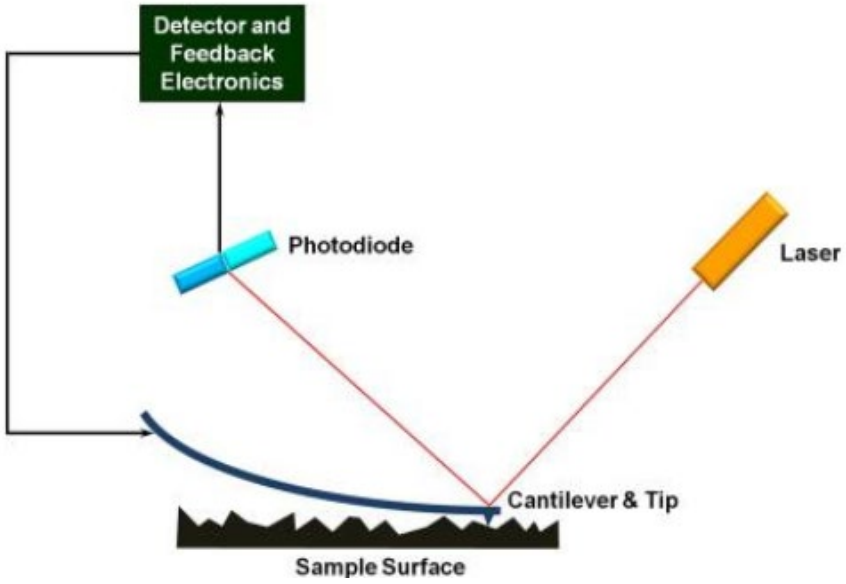

Figure I.3. Schematic diagram of a typical AFM instrument **[103].**

I.1.4.2. SEM morphology of the MZO thin films

Essential information about the surface morphology of the sample can be produced from Scanning Electron Microscopy (SEM) analysis**.** The electron beam of SEM interacts with atoms at different depths within the sample and emits X-rays, backscattered electrons, secondary electrons, and Auger electrons. SEM makes use of the backscattered and the secondary electrons and produces High-resolution images (**Figure I.4)**. The obstacle created by the vaporized water in the vacuum, obscures the clarity of the image. So, removal of water is essential **[110]**. Coating of non-conducting or poorly conducting thin films by conductive layer of metal (Typical range of 2–20 nm) is required in SEM to enable or improve the imaging. This process reduces thermal damage and charging and improves the secondary electron emission **[110, 111]**.

Many reports showed SEM images for MZO films elaborated by different process at various experimental conditions**[28, 82, 98, 108, 112]**. FE-SEM images of MZO thin films with Mn content of 1, 2 and 5at **[67]** . For 1 at% Mn, the films consist of equiaxed nanoparticles with an average diameter of around 50 nm. At 2 at% Mn, the films show a more compact and uniform structure with slightly reduced grain size, indicating improved densification. For 5 at%

Mn, the grain size further decreases and the surface becomes even smoother with lesser overgrown particles, suggesting enhanced film uniformity and suppressed grain growth at higher Mn concentrations.

In their study on Mn doping, Dan et al**[68]**. reported that SEM analysis revealed compact, crack-free surfaces in both undoped and Mn-doped ZnO thin films. The nanorod diameter was observed to decrease with increasing Mn doping level. At 7 at%, the structures showed enhanced uniformity and noticeable morphological variation, MZO films with $0 \leq x \leq 7$ at% displayed aligned and dense nanorods at low doping, which transformed into irregular microstructures at higher *x* **[95]**.

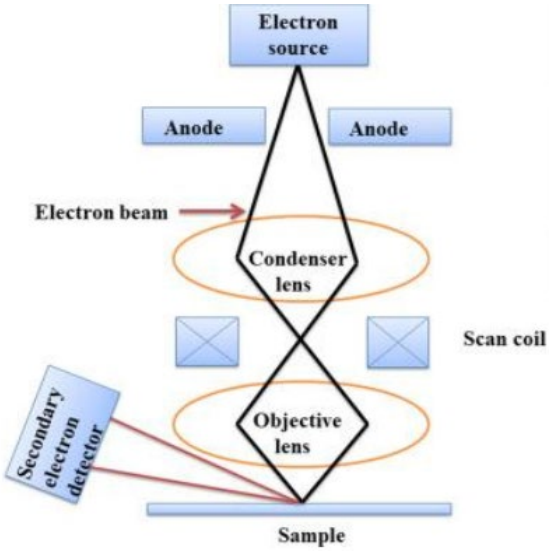

Figure I.4. Schematic diagram of Scanning Electron Microscopy (SEM) **[110]**.

From findings on morphology analysis either by AFM or by SEM microscopy, one can draw the following remarks,

- **i.** Mn doping and particle form: the particle shape and size are significantly affected by the Mn doping level, with noticeable morphological transitions,
- **ii.** Mn doping and grains density: increasing Mn content generally leads to denser and more compact grain structures,
- **iii.** Mn doping and roughness: surface roughness shows varying trends with Mn doping depending on synthesis conditions,
- **iv.** Mn doping and internal structure: higher Mn concentrations can result in suppressed grain growth and morphological changes in the MZO thin films.

I.1.5. Electronic and optical properties of MZO thin films

I.1.5.1. Transmittance and band gap energy

Analysis by Ultraviolet-Visible (UV-Vis) spectroscopy is an important tool used to characterize materials by light in ultraviolet (UV: ~300 -400 nm), visible (Vis: ~400-750 nm), and near infrared ranges (NIR: ~750-3200 nm). The measured spectra of MZO thin films deposited on transparent substrates may be received as transmittance, absorbance or reflectance of radiation and quantitative and qualitative information are then provided. For MZO thin films, the band gap absorption was found to vary in the ultraviolet region while the main optical parameter, i.e. static refractive index, was estimated from the interference fringes of the optical transmission spectrum in the visible and ultraviolet ranges.

Ellipsometry, with non-normal incidence of light, and the spectral reflectance, with the incident light perpendicular to the film surface, are two most common optical measurement types. This latter is generally much simpler and suitable for MZO transparent thin films. UV-Vis spectroscopy has been commonly used as suitable method to characterize the optical and electronic properties of MZO thin films deposited on transparent substrates **[21, 23, 112]** from measurement of transmittance and/or reflectance. Optical energy gap E_g can then be extracted using the well-known Tauc relationship **[113]**. The dispersive refractive index spectrum in photon energy range less than E_g are analyzed by Wemple and DiDomenico according to the single-efiective-oscillator model **[114]**. For basic UV-vis characterization, the MZO thin film sample is placed accordingly with a double-beam UV-Vis spectrophotometer (**Figure I.5**) **[115]**. The reference cell often contains the substrate (utilized as a reference) and the other cell

contains the sample (MZO thin film). The spectrum of MZO thin film is then obtained by subtracting the absorbance of the substrate.

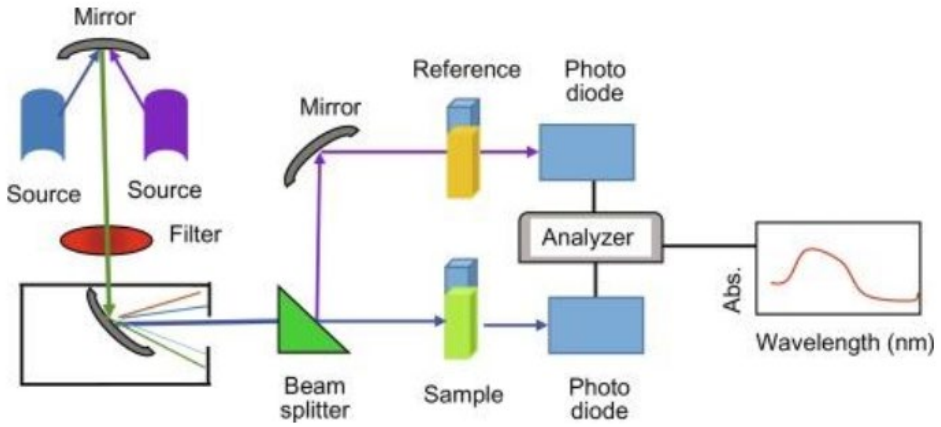

Figure I.5. A schematic diagram of a double-beam UV-Vis spectrophotometer **[115]**.

MZO thin films generally exhibited high optical transmittance in the higher wavelength region (λ≥400 nm)**[30, 112, 116]**. The shift in the absorption edge in the transmittance spectra of MZO thin films towards lower wavelength region are observed with increasing of Mn concentration **[31]**. For a uniform film, the interference effects give rise to oscillating curves (interference fringes), which are used to estimate the optical parameters, such as refractive index, and the thickness of the films. These interference fringes disappear in the region of strong absorption (λ≤400 nm) and they are not usually observed for films with very low thickness.

The average transmittance in the visible region was found to be influenced by increasing Mn doping**[77, 78]**. Some reports found that average transmittance is decreased with increasing Mn content**[21, 116]**. whereas Some studies reported that as the film thickness increased, the average optical transmittance decreased due to increased light scattering and absorption, although the actual absorption coefficient may be reduced due to structural defects such as cracks**[21, 28]**. To justify these trends, various causes have been given, The slight improvement in the average transmittance for pure and MZO thin films of 5, 10, 15 and 0.7 and 20 layers, was attributed to the optical scattering**[28]**. This scattering was decreased by the reducing in the density of grain boundary, which stems from the increased grain size. In other work for pure and MZO thin films with Mn content of 0.05 and 0.1 mol% **[117],** authors explained the slight decrease with Mn content by the creation of oxygen vacancies and scattering at the grain boundaries**[67]**.

The band gap (Eg) values of the MZO thin films at different Mn contents was obtained from measured transmittance and/or absorbance**[68, 116, 118].** The observed shift in the

absorption edge in the transmittance spectra towards higher wavelength region suggests the shrinking of the band gap energy**.** The broadening of the band gap energy was noticed in few reports**[119]**. On the other hand, this may be attributed to the s–d and p–d interactions to explain the narrowing of the band gap with Mn concentration observed**[69]**. Sivalingam et al. **[98]** reported that this trend may be due to the manifestation of the presence of strong exchange interaction between localized d electron of Mn^{2+} ion and the s and p electrons of host matrix (ZnO). This can also be theoretically explained using the second-order perturbation theory **[98, 120].**

Finally, it is worth noting to provide the reader by a summary of the main findings on the transmittance and bandgap for MZO thin films:

a) Shift in absorption edge: A shift of the absorption edge towards lower wavelengths was observed with increasing Mn concentration, indicating a broadening or shrinking of the bandgap depending on the nature of Mn interaction.
b) Average transmittance trend: The average transmittance decreased with increasing Mn doping and/or film thickness, due to enhanced light scattering and absorption, as well as grain boundary effects and oxygen vacancies.
c) Shrinking of bandgap: The narrowing of the bandgap with Mn content was attributed to s–d and p–d exchange interactions between Mn^{2+} ions and the ZnO host matrix, which may be explained theoretically via second-order perturbation theory.

I.1.10. Conclusion and prospectus/future/outlook

Various studies have been carried out on the investigation of MZO thin films in view of various applications. A summary of structural, electronic and optical parameters of MZO thin films was tabulated in order to investigate their evolution by increasing level of Mn content under variety of experimental conditions. It was found that each combination solvent-precursors-additive under various experimental conditions as well as the elaboration method strongly affects the various properties of elaborated MZO thin films. The crystallite size, lattice constants, lattice strain, diffraction peaks, band gap, transmittance, and surface morphology, were found to be influenced by increasing Mn doping. Moreover, various experiments with the same Mn content led to results possessing a contradictory evolution. This confirmed the effect of the involved experimental parameters on the growth and structured of MZO thin films.

Best knowledge on the combined effects of the preparation method and conditions as well as adding material, i.e. Mn, help in exploring a variety of new potential applications for MZO thin films. So, further researches are required to produce homogenous incorporation of Mn dopant into ZnO host lattice and to gain more insights into the MZO preparation-property-application relationship. We hope to provide support in the area of elaboration process, characterization and properties of low thickness metal oxides thin films and our review can open the door to researchers working on MZO thin films elaboration to improve their performance for the typical applications, like gas sensing and optoelectronic devices technology, or even to exploring new applications in technological devices.

References

[1] J.-B. Lee, M.-H. Lee, C.-K. Park, and J.-S. Park, "Effects of lattice mismatches in ZnO/substrate structures on the orientations of ZnO films and characteristics of SAW devices," *Thin solid films,* vol. 447, pp. 296-301, 2004.

[2] D. Borah, M. K. Baruah, P. P. Saikia, K. K. Senapoty, M. Barua, and R. Singha, "Structural characterization and surface environment of ZnO nanoflowers," *Journal of Material and Environmental Science,* vol. 7, pp. 310-315, 2016.

[3] A. M. Díez-Pascual, "Biodegradable food packaging nanocomposites based on ZnO-reinforced polyhydroxyalkanoates," in *Food Packaging*: Elsevier, 2017, pp. 185-221.

[4] A. R. Nimbalkar and M. G. Patil, "Synthesis of highly selective and sensitive Cu-doped ZnO thin film sensor for detection of H2S gas," *Materials Science in Semiconductor Processing,* vol. 71, pp. 332-341, 2017, Art no. 22.

[5] S. Guo, Q. Hou, C. Zhao, and Y. J. C. P. L. Zhang, "Study of the effect of Cu heavy doping on band gap and absorption spectrum of ZnO," vol. 614, pp. 15-20, 2014.

[6] P. Liu, Y. Guo, Q. Xu, F. Wang, Y. Li, and K. Shao, "Enhanced photocatalytic performance of ZnO/multi-walled carbon nanotube nanocomposites for dye degradation," *Ceramics International,* vol. 40, no. 4, pp. 5629-5633, 2014.

[7] H. Yin and P. S. Casey, "ZnO nanorod composite with quenched photoactivity for UV protection application," *Materials Letters,* vol. 121, pp. 8-11, 2014.

[8] T. Ootsuka *et al.*, "Studies on aluminum-doped ZnO films for transparent electrode and antireflection coating of β-FeSi2 optoelectronic devices," *Thin Solid Films,* vol. 476, no. 1, pp. 30-34, 2005.

[9] C. Jagadish and S. J. Pearton, *Zinc oxide bulk, thin films and nanostructures: processing, properties, and applications*. Elsevier, 2011.

[10] J. M. Szarko *et al.*, "Optical injection probing of single ZnO tetrapod lasers," *Chemical physics letters,* vol. 404, no. 1-3, pp. 171-176, 2005.

[11] M. Karyaoui *et al.*, "Some physical investigations on silver-doped ZnO sprayed thin films," *Materials Science in Semiconductor Processing,* vol. 30, pp. 255-262, 2015.

[12] N. Narayanan and N. K. Deepak, "Enhancement of visible luminescence and photocatalytic activity of ZnO thin films via Cu doping," *Optik,* vol. 158, pp. 1313-1326, 2018, doi: 10.1016/j.ijleo.2018.01.024.

[13] C.-C. Yu, W.-H. Lan, and K.-F. Huang, "Indium-nitrogen codoped zinc oxide thin film deposited by ultrasonic spray pyrolysis on n-(111) Si substrate: the effect of film thickness," *Journal of Nanomaterials,* vol. 2014, 2014.

[14] Y.-F. Hsiou, W.-K. Hung, and C.-W. Wang, "Fabrication of Sb-doped p-type ZnO thin films by pulsed laser deposition," *Atlas Journal of Materials Science,* vol. 2, no. 1, pp. 60-64, 2015.

[15] V. Şenay *et al.*, "ZnO thin film synthesis by reactive radio frequency magnetron sputtering," *Applied surface science,* vol. 318, pp. 2-5, 2014.

[16] T. Morita *et al.*, "Fabrication of transparent ZnO thick film with unusual orientation by the chemical bath deposition," *Crystal Growth & Design,* vol. 15, no. 7, pp. 3150-3156, 2015.

[17] J.-C. Hsiao *et al.*, "Highly textured ZnO: B films grown by low pressure chemical vapor deposition for efficiency enhancement of heterojunction silicon-based solar cells," *Journal of the Taiwan Institute of Chemical Engineers,* vol. 44, no. 5, pp. 758-761, 2013.

[18] G. Poongodi, P. Anandan, R. M. Kumar, and R. Jayavel, "Studies on visible light photocatalytic and antibacterial activities of nanostructured cobalt doped ZnO thin films prepared by sol–gel spin coating method," *Spectrochimica Acta Part A: Molecular and Biomolecular Spectroscopy,* vol. 148, pp. 237-243, 2015.

[19] R. Hussin, H. Yahya, and N. Zulkiflee, "Depositionof TiO 2/ZnO Thin Films Using Spin-Coating Method," *Int. J. Curr. Res. Sci. Eng. Technol,* vol. 1, no. 226, pp. 2018.226-232, 2018.

[20] D. Akcan, A. Gungor, and L. Arda, "Structural and optical properties of Na-doped ZnO films," *Journal of Molecular structure,* vol. 1161, pp. 299-305, 2018.

[21] X. Li, X. Zhu, and K. Jin, "Study on structural and optical properties of Mn-doped ZnO thin films by sol-gel method," *Optical Materials,* vol. 100, p. 109657, 2020.
[22] C. Belkhaoui, N. Mzabi, H. Smaoui, and P. Daniel, "Enhancing the structural, optical and electrical properties of ZnO nanopowders through (Al+ Mn) doping," *Results in Physics,* vol. 12, pp. 1686-1696, 2019.
[23] S. Ahmed, "Structural, optical, and magnetic properties of Mn-doped ZnO samples," *Results in physics,* vol. 7, pp. 604-610, 2017.
[24] K. Karthika and K. Ravichandran, "Enhancing the magnetic and antibacterial properties of ZnO nanopowders through Mn+ Co doping," *Ceramics International,* vol. 41, no. 6, pp. 7944-7951, 2015.
[25] J. C. Fan, K. Sreekanth, Z. Xie, S. Chang, and K. V. J. P. i. M. S. Rao, "p-Type ZnO materials: Theory, growth, properties and devices," vol. 58, no. 6, pp. 874-985, 2013.
[26] L. Zhu, W. J. S. Zeng, and A. A. Physical, "Room-temperature gas sensing of ZnO-based gas sensor: A review," vol. 267, pp. 242-261, 2017.
[27] B. L. Martínez-Vargas *et al.*, "Synthesis and characterization of n-ZnO/p-MnO nanocomposites for the photocatalytic degradation of anthracene," *Journal of Photochemistry and Photobiology A: Chemistry,* vol. 369, pp. 85-96, 2019.
[28] A. Boukhari *et al.*, "Thickness effect on the properties of Mn-doped ZnO thin films synthesis by sol-gel and comparison to first-principles calculations," *Ceramics International,* vol. 47, no. 12, pp. 17276-17285, 2021.
[29] S. Prasad, V. Kumar, S. Kirubanandam, and A. Barhoum, "Engineered nanomaterials: nanofabrication and surface functionalization," in *Emerging Applications of Nanoparticles and Architecture Nanostructures*: Elsevier, 2018, pp. 305-340.
[30] M. Sharma, K. Bera, R. Mishra, and A. V. Kuanr, "Structural, magnetic, and optical properties of Mn2+ doping in ZnO thin films," *Surfaces,* vol. 4, no. 4, pp. 268-278, 2021.
[31] A. Rahal *et al.*, "Experimental investigation of structural and optical properties of Mn-doped ZnO thin films deposited by pneumatic spray technique," *Scientific Reports,* vol. 15, no. 1, p. 7086, 2025.
[32] B. D. Naorem *et al.*, "Mn-doped ZnO thin films as a platform for reagentless uric acid biosensor," *Chemical Physics Impact,* vol. 10, p. 100823, 2025.
[33] S. Goktas, A. Tumbul, and A. Goktas, "Growth technique–induced highly C-axis-oriented ZnO: Mn, Zno: Fe and ZnO: Co thin films: a comparison of nanostructure, surface morphology, optical band gap, and room Temperature ferromagnetism," *Journal of Superconductivity and Novel Magnetism,* vol. 36, no. 10, pp. 1875-1892, 2023.
[34] F. Lekoui *et al.*, "Investigation of annealing environment effect on the structural, morphological, and linear/nonlinear optical properties of nanostructured Mn-doped ZnO thin films," *Inorganic Chemistry Communications,* vol. 176, p. 114209, 2025.
[35] Á. P. Lanchero, L. F. Prieto, H. P. Quiroz, J. A. Calderón, A. Dussan, and F. Mesa, "Impact of Mn/Co substitution on magnetoelectric and structural properties of ZnO nanostructures thin films," *Heliyon,* 2025.
[36] S. J. V. Aydemir, "Effects of withdrawal speed on the microstructural and optical properties of sol–gel grown ZnO: Al thin films," vol. 120, pp. 51-58, 2015.
[37] A. Mahroug, R. Amari, A. Boukhari, B. Deghfel, L. Guerbous, and N. Selmi, "Synthesis, structural, morphological, electronic, optical and luminescence properties of pure and manganese-doped zinc oxide nanostructured thin films: effect of doping," *Journal of Nanoelectronics and Optoelectronics,* vol. 13, no. 5, pp. 732-742, 2018.
[38] L. L. Hench and J. K. West, "The sol-gel process," *Chemical reviews,* vol. 90, no. 1, pp. 33-72, 1990.
[39] N. Al-Dahoudi, "Wet chemical deposition of transparent conducting coatings made of redispersable crystalline ITO nanoparticles on glass and polymeric substrates," 2003.
[40] S. D. Ponja, "Metal oxide thin films for optoelectronic applications," UCL (University College London), 2018.

[41] A. Ali Fatima, S. Devadason, and T. Mahalingam, "Structural, luminescence and magnetic properties of Mn doped ZnO thin films using spin coating technique," *Journal of Materials Science: Materials in Electronics,* vol. 25, pp. 3466-3472, 2014.

[42] M. Çavaş, "Investigation morphological, electrical, and optical properties of Mn-doped ZnO thin film by sol–gel spin-coating method," *Journal of Theoretical and Applied Physics,* vol. 11, pp. 325-331, 2017.

[43] Z. Gültekin, M. Alper, M. C. Hacıismailoğlu, and C. Akay, "Effect of Mn doping on structural, optical and magnetic properties of ZnO films fabricated by sol–gel spin coating method," *Journal of Materials Science: Materials in Electronics,* vol. 34, no. 5, p. 438, 2023.

[44] P. Thamaraiselvan, S. Kannan, P. Gowthaman, and M. Kutraleeswaran, "Preparation and Characterization of Mn Doped Zno Nanoparticles," *Int. JS Res. Sci. Tech,* vol. 4, pp. 679-685, 2018.

[45] A. Kharoubi *et al.*, "Sol–gel dip coating method synthesis of Mn-doped titanium dioxide thin films," *Journal of Molecular and Engineering Materials,* vol. 6, no. 01n02, p. 1850001, 2018.

[46] C. Busuioc, S. I. Jinga, and E. Andronescu, "FILME SUBTIRI PE BAZA DE TANTALAT DE BARIU SI MAGNEZIU OBTINUTE PRIN PROCESARE SOL-GEL/BARIUM MAGNESIUM TANTALATE THIN FILMS OBTAINED BY SOL-GEL PROCESSING," *Revista Romana de Materiale,* vol. 42, no. 3, p. 299, 2012.

[47] M. Aymerich, A. I. Gómez-Varela, E. Álvarez, and M. T. Flores-Arias, "Study of different sol-gel coatings to enhance the lifetime of PDMS devices: evaluation of their biocompatibility," *Materials,* vol. 9, no. 9, p. 728, 2016.

[48] S. Thiagarajan, A. Sanmugam, and D. J. R. A. i. S.-G. S. Vikraman, "Facile methodology of sol-gel synthesis for metal oxide nanostructures," pp. 1-17, 2017.

[49] F. Dabir, H. Esfahani, F. Bakhtiargonbadi, and Z. Khodadadi, "Study on microstructural and electro-optical properties of sol–gel derived pure and Al/Cu-doped ZnO thin films," *Journal of Sol-Gel Science and Technology,* pp. 1-10, 2020.

[50] D. V. Vu, D. H. Le, T. T. Nguyen, T. Van Duong, Q. D. Ngo, and T. Q. Trinh, "Study on material properties of Sn-and Cu-doped ZnO thin films as n-and p-type thermoelectric materials based on wet solution synthesis," *Journal of Materials Science: Materials in Electronics,* vol. 30, no. 7, pp. 6544-6551, 2019.

[51] E. Asikuzun, O. Ozturk, L. Arda, and C. Terzioglu, "Preparation, growth and characterization of nonvacuum Cu-doped ZnO thin films," *Journal of Molecular Structure,* vol. 1165, pp. 1-7, 2018.

[52] V. Ganesh, G. Salem, I. Yahia, and F. Yakuphanoglu, "Synthesis, optical and photoluminescence properties of Cu-doped ZnO nano-fibers thin films: nonlinear optics," *Journal of Electronic Materials,* vol. 47, no. 3, pp. 1798-1805, 2018.

[53] K. Joshi, M. Rawat, S. K. Gautam, R. Singh, R. Ramola, and F. Singh, "Band gap widening and narrowing in Cu-doped ZnO thin films," *Journal of Alloys and Compounds,* vol. 680, pp. 252-258, 2016.

[54] S. Horzum, E. Torun, T. Serin, and F. Peeters, "Structural, electronic and optical properties of Cu-doped ZnO: experimental and theoretical investigation," *Philosophical Magazine,* vol. 96, no. 17, pp. 1743-1756, 2016.

[55] H. Gómez-Pozos *et al.*, "Cu-doped ZnO thin films deposited by a sol-gel process using two copper precursors: gas-sensing performance in a propane atmosphere," *Materials,* vol. 9, no. 2, p. 87, 2016.

[56] T. Saidani, M. Zaabat, M. Aida, and B. Boudine, "Effect of copper doping on the photocatalytic activity of ZnO thin films prepared by sol–gel method," *Superlattices and Microstructures,* vol. 88, pp. 315-322, 2015.

[57] K. Poornima, K. G. Krishnan, B. Lalitha, and M. Raja, "CdS quantum dots sensitized Cu doped ZnO nanostructured thin films for solar cell applications," *Superlattices and Microstructures,* vol. 83, pp. 147-156, 2015.

[58] M. Raja, N. Muthukumarasamy, D. Velauthapillai, and R. Balasundaraprabhu, "Influence of copper on the morphology and properties of one dimensional ZnO nanorod structures," *Superlattices and Microstructures,* vol. 72, pp. 102-110, 2014.

[59] K. Chongsri, S. Aunpang, W. Techitdheera, and W. Pecharapa, "Preparation and characterization of Cu-doped ZnO sol-gel derived optical thin films," in *Advanced Materials Research*, 2013, vol. 802: Trans Tech Publ, pp. 124-128.

[60] H. Yang *et al.*, "Effects of dopants on magnetic properties of Cu-doped ZnO thin films," *Journal of Materials Science,* vol. 47, no. 1, pp. 530-533, 2012.

[61] K. Ranjith, K. Vanishri, and R. Rajendrakumar, "Synthesis and catalytic properties of Al and Cu doped ZnO thin films on the photolytic degradation of methylene blue," *Synthesis and Reactivity in Inorganic, Metal-Organic, and Nano-Metal Chemistry,* vol. 44, no. 9, pp. 1316-1322, 2014.

[62] P. Jongnavakit, P. Amornpitoksuk, S. Suwanboon, and N. Ndiege, "Preparation and photocatalytic activity of Cu-doped ZnO thin films prepared by the sol–gel method," *Applied Surface Science,* vol. 258, no. 20, pp. 8192-8198, 2012.

[63] J. Wojnarowicz *et al.*, "Structural and magnetic properties of Co–Mn codoped ZnO nanoparticles obtained by microwave solvothermal synthesis," *Crystals,* vol. 8, no. 11, p. 410, 2018.

[64] Z. Mickovic, "Study of diluted magnetic semiconductors: The case of transition metal doped ZnO," EPFL, 2010.

[65] C. Jing, Y. Jiang, W. Bai, J. Chu, and A. Liu, "Synthesis of Mn-doped ZnO diluted magnetic semiconductors in the presence of ethyl acetoacetate under solvothermal conditions," *Journal of magnetism and magnetic materials,* vol. 322, no. 16, pp. 2395-2400, 2010.

[66] L. R. M. Reddy, "COMPOSITION, OPTICAL AND PL PROPERTIES OF Mn DOPED ZnO NANO CRYSTALLINE THIN FILMS PREPARED BY SOL-GEL METHOD," 2019.

[67] C. M. Vladut *et al.*, "Optical and Piezoelectric Properties of Mn-Doped ZnO Films Deposited by Sol-Gel and Hydrothermal Methods," *Journal of Nanomaterials,* vol. 2019, no. 1, p. 6269145, 2019.

[68] D. Hu *et al.*, "Structural and optical properties of Mn-doped ZnO nanocrystalline thin films with the different dopant concentrations," *Physica E: Low-dimensional Systems and Nanostructures,* vol. 61, pp. 14-22, 2014.

[69] D. Sivalingam, J. B. Gopalakrishnan, and J. B. B. Rayappan, "Structural, morphological, electrical and vapour sensing properties of Mn doped nanostructured ZnO thin films," *Sensors and Actuators B: Chemical,* vol. 166, pp. 624-631, 2012.

[70] R. Karmakar, S. Neogi, A. Banerjee, and S. Bandyopadhyay, "Structural; morphological; optical and magnetic properties of Mn doped ferromagnetic ZnO thin film," *Applied surface science,* vol. 263, pp. 671-677, 2012.

[71] A. Abd Rashid and P. Menon, "Effect of Mn doping on the structural and optical properties of ZnO films," in *2010 IEEE International Conference on Semiconductor Electronics (ICSE2010)*, 2010: IEEE, pp. 79-82.

[72] Z. B. Bahşi and A. Y. Oral, "Effects of Mn and Cu doping on the microstructures and optical properties of sol–gel derived ZnO thin films," *Optical Materials,* vol. 29, no. 6, pp. 672-678, 2007.

[73] A. H. Rakhsha, H. Abdizadeh, E. Pourshaban, M. R. Golobostanfard, V. R. Mastelaro, and M. J. M. Montazerian, "Ag and Cu doped ZnO nanowires: A pH-Controlled synthesis via chemical bath deposition," vol. 5, p. 100212, 2019.

[74] U. Maiti, P. Ghosh, S. Nandy, and K. Chattopadhyay, "Effect of Mn doping on the optical and structural properties of ZnO nano/micro-fibrous thin film synthesized by sol–gel technique," *Physica B: Condensed Matter,* vol. 387, no. 1-2, pp. 103-108, 2007.

[75] K. Chebbah *et al.*, "Structural and optical properties of N and Mn co-doped ZnO thin films grown by ultrasonic spray pyrolysis method," *Journal of Nanoelectronics and Optoelectronics,* vol. 14, no. 1, pp. 39-49, 2019.

[76] M. Sima, T. Visan, E. Matei, F. Ungureanu, I. Enculescu, and M. Sima, "Electrochemical Growth of Eosin Y/Manganese Doped ZnO as Hybrid Films and Nanowires," *Zeitschrift für Physikalische Chemie,* vol. 225, no. 3, pp. 325-339, 2011.

[77] A. Aravind, M. Jayaraj, M. Kumar, and R. Chandra, "Structural, optical and magnetic properties of Mn doped ZnO thin films prepared by pulsed laser deposition," *Materials science and Engineering: B,* vol. 177, no. 13, pp. 1017-1022, 2012.

[78] S. Yang and Y. Zhang, "Structural, optical and magnetic properties of Mn-doped ZnO thin films prepared by sol–gel method," *Journal of magnetism and magnetic materials,* vol. 334, pp. 52-58, 2013.

[79] M. Ghazi, M. Izadifard, F. E. Ghodsi, and M. Yuonesi, "Studying Mn-and Ni-doped ZnO thin films synthesized by the sol–gel method," *Journal of superconductivity and novel magnetism,* vol. 25, pp. 101-108, 2012.

[80] A. Rana *et al.*, "Studies of optoelectrical properties of Mn-doped ZnO nanostructure for supercapacitor and photodetector applications," *Journal of Alloys and Compounds,* vol. 997, p. 174931, 2024.

[81] F. Dabir, H. Esfahani, F. Bakhtiargonbadi, and Z. Khodadadi, "Study on microstructural and electro-optical properties of sol–gel derived pure and Al/Cu-doped ZnO thin films," *Journal of Sol-Gel Science and Technology,* vol. 96, pp. 529-538, 2020.

[82] S. Mondal, S. Bhattacharyya, and P. Mitra, "Preparation of manganese-doped ZnO thin films and their characterization," *Bulletin of Materials Science,* vol. 36, pp. 223-229, 2013.

[83] A. López-Suárez, D. Acosta, C. Magaña, and F. Hernández, "Optical, structural and electrical properties of ZnO thin films doped with Mn," *Journal of Materials Science: Materials in Electronics,* vol. 31, no. 10, pp. 7389-7397, 2020.

[84] A. Renitta and K. Vijayalakshmi, "High performance hydrogen sensor based on Mn implanted ZnO nanowires array fabricated on ITO substrate," *Materials Science and Engineering: C,* vol. 77, pp. 245-256, 2017.

[85] F. Li, M. Zhang, G. Hou, Y. Shen, Z. Liu, and H. Li, "Sol-gel preparation and phosphorescence property of Mn 2+-doped zinc borosilicate glass thin films," *Rare Metals,* vol. 30, pp. 298-303, 2011.

[86] L. Znaidi, "Sol–gel-deposited ZnO thin films: A review," *Materials Science and Engineering: B,* vol. 174, no. 1-3, pp. 18-30, 2010.

[87] A. Pathak, A. Soni, A. Chaudhary, and U. Deshpande, "The Influence of Manganese Doping on Zinc Oxide Nanoparticles for Photocatalytic Degradation of Methylene Blue Dye," *Eurasian Journal of Analytical Chemistry,* vol. 19, no. 1, 2024.

[88] Y. Xi *et al.*, "In-situ stress gradient evolution and texture-dependent fracture of brittle ceramic thin films under external load," vol. 44, no. 7, pp. 8176-8183, 2018.

[89] S. K. Kundara *et al.*, "Tailoring the structural, optical and electrical properties of Mn doped ZnO thin films for gas sensing response," *Science of Advanced Materials,* vol. 15, no. 6, pp. 772-780, 2023.

[90] M. Kaliva and M. Vamvakaki, "Chapter 17 - Nanomaterials characterization," in *Polymer Science and Nanotechnology*, R. Narain Ed.: Elsevier, 2020, pp. 401-433.

[91] A. Mhamdi, R. Mimouni, A. Amlouk, M. Amlouk, and S. Belgacem, "Study of copper doping effects on structural, optical and electrical properties of sprayed ZnO thin films," *Journal of Alloys and Compounds,* vol. 610, pp. 250-257, 2014, doi: 10.1016/j.jallcom.2014.04.007.

[92] S. Yang, Y. Zhang, and D. Mo, "Spectroscopic ellipsometry studies of sol-gel-derived Cu-doped ZnO thin films," *Thin Solid Films,* vol. 571, pp. 605-608, 2014, doi: 10.1016/j.tsf.2014.02.097.

[93] M. Salem, I. Massoudi, S. Akir, Y. Litaiem, M. Gaidi, and K. Khirouni, "Photoelectrochemical and opto-electronic properties tuning of ZnO films: Effect of Cu doping content," *Journal of Alloys and Compounds,* vol. 722, pp. 313-320, 2017.

[94] R. Siddheswaran, C. E. Jeyanthi, K. Thangaraju, and R. Mangalaraja, "Columnar structure growth of Mn-doped ZnO (MZO) thin films by radio frequency co-sputtering and studies on films properties," *Materials Technology,* vol. 37, no. 2, pp. 79-85, 2022.

[95] P. Soundarrajan and K. Sethuraman, "Interface energy barrier tailoring the morphological structure evolution from ZnO nano/micro rod arrays to microcrystalline thin films by Mn doping," *RSC Advances,* vol. 5, no. 55, pp. 44222-44233, 2015.

[96] S. Fabbiyola, L. J. Kennedy, A. Dakhel, M. Bououdina, J. J. Vijaya, and T. Ratnaji, "Structural, microstructural, optical and magnetic properties of Mn-doped ZnO nanostructures," *Journal of Molecular Structure,* vol. 1109, pp. 89-96, 2016.

[97] M. Kumar *et al.*, "Synthesis, characterization, photocatalytic and sensing properties of Mn-Doped ZnO nanoparticles," *Journal of Nanoscience and Nanotechnology,* vol. 19, no. 12, pp. 8095-8103, 2019.

[98] P. Singh, A. Kaushal, and D. Kaur, "Mn-doped ZnO nanocrystalline thin films prepared by ultrasonic spray pyrolysis," *Journal of Alloys and Compounds,* vol. 471, no. 1-2, pp. 11-15, 2009.

[99] M. Habibi and M. K. Sardashti, "BStructure and morphology of nanostructured Zinc oxide thin films prepared by dip vs. spin-coating methods,[J," *Iran. Chem. Soc,* vol. 5, no. 4, pp. 603-609, 2008.

[100] A. Dhanalakshmi, S. Thanikaikarasan, and B. Natarajan, "Influence of Mn dopant concentration on film thickness, structural, morphological, compositional and optical properties of zinc oxide thin films," *Journal of Materials Science: Materials in Electronics,* vol. 28, pp. 11576-11583, 2017.

[101] U. Ilyas *et al.*, "Quenching of surface traps in Mn doped ZnO thin films for enhanced optical transparency," *Applied Surface Science,* vol. 258, no. 2, pp. 890-897, 2011.

[102] Q. Gao, Y. Dai, X. Li, L. Yang, C. Cui, and C. Li, "Effects of Mn dopant on tuning carrier concentration in Mn doped ZnO nanoparticles synthesized by co-precipitation technique," *Journal of Materials Science: Materials in Electronics,* vol. 29, pp. 3568-3575, 2018.

[103] H. Wang and P. K. Chu, "Surface characterization of biomaterials," in *Characterization of biomaterials*: Elsevier, 2013, pp. 105-174.

[104] G. Qian, Y. Li, and A. R. J. S. S. R. Gerson, "Applications of surface analytical techniques in Earth Sciences," vol. 70, no. 1, pp. 86-133, 2015.

[105] S. Ebrahimi, B. Yarmand, and N. Naderi, "High-performance UV-B detectors based on MnxZn1-xS thin films modified by bandgap engineering," *Sensors and Actuators A: Physical,* vol. 303, p. 111832, 2020.

[106] M. V. Gallegos, M. A. Peluso, H. Thomas, L. C. Damonte, and J. E. Sambeth, "Structural and optical properties of ZnO and manganese-doped ZnO," *Journal of Alloys and Compounds,* vol. 689, pp. 416-424, 2016.

[107] Y. Wang, X. Hao, Z. Wang, M. Dong, and L. Cui, "Facile fabrication of Mn2+-doped ZnO photocatalysts by electrospinning," *Royal Society Open Science,* vol. 7, no. 4, p. 191050, 2020.

[108] M. Faraz, M. Z. Ansari, and N. Khare, "Synthesis of nanostructure manganese doped zinc oxide/polystyrene thin films with excellent stability, transparency and super-hydrophobicity," *Materials Chemistry and Physics,* vol. 211, pp. 137-143, 2018.

[109] C. Ma, W. Wang, S. Li, C. Miao, and Q. Zhang, "Multifractal, structural, and optical properties of Mn-doped ZnO films," *Applied surface science,* vol. 261, pp. 231-236, 2012.

[110] D. Titus, E. J. J. Samuel, and S. M. Roopan, "Nanoparticle characterization techniques," in *Green Synthesis, Characterization and Applications of Nanoparticles*: Elsevier, 2019, pp. 303-319.

[111] A. S. H. Makhlouf and H. Soliman, "Effect of nano-additives (Al2O3 and NaF) on the performance of ceramic coatings formed by microarc oxidation on magnesium alloys," in *Handbook of Nanoceramic and Nanocomposite Coatings and Materials*: Elsevier, 2015, pp. 389-401.

[112] E. Benrezgua *et al.*, "Synthesis of low-content Mn-doped ZnO thin films: Characterizations and density functional theory studies," *Inorganic Chemistry Communications,* vol. 172, p. 113710, 2025.

[113] H. Fritzsche and J. J. P. P. Tauc, New York,) p, "Amorphous and liquid semiconductors," vol. 254, 1974.
[114] S. Wemple and M. J. P. R. B. DiDomenico Jr, "Behavior of the electronic dielectric constant in covalent and ionic materials," vol. 3, no. 4, p. 1338, 1971.
[115] J. E. House, *Fundamentals of quantum mechanics*. Academic Press, 2017.
[116] Q. Xie, X. Liu, and H. Liu, "Fastly steady UV response feature of Mn-doped ZnO thin films," *Superlattices and Microstructures,* vol. 139, p. 106391, 2020.
[117] S. Syed Zahirullah, J. Joseph Prince, and P. Fermi Hilbert Inbaraj, "Structural and optical properties of Cu-doped ZnO nanorods by silar method," *Materials technology,* vol. 32, no. 12, pp. 755-763, 2017, Art no. 15.
[118] M. Xin, L. Z. Hu, D.-P. Liu, and N.-S. Yu, "Effect of Mn doping on the optical, structural and photoluminescence properties of nanostructured ZnO thin film synthesized by sol–gel technique," *Superlattices and Microstructures,* vol. 74, pp. 234-241, 2014.
[119] G. Rusu, P. Gorley, C. Baban, A. Rambu, and M. Rusu, "Preparation and characterization of Mn-doped ZnO thin films," *Journal of Optoelectronics and Advanced Materials,* vol. 12, no. 4, p. 895, 2010.
[120] R. Bylsma, W. Becker, J. Kossut, U. Debska, and D. Yoder-Short, "Dependence of energy gap on x and T in Zn 1− x Mn x Se: the role of exchange interaction," *Physical Review B,* vol. 33, no. 12, p. 8207, 1986.

CHAPTER II:

Metal Oxides Nanomaterials and Experimental Background

II.1. Metal oxides nanomaterials

II.1.1. Introduction

Thin film technology is both an ancient art and a relatively new science. The use of thin films extends back to the metal ages of antiquity **[1]**. In recent years, many researchers have focused on studying the properties of thin films due to the easy and versatility of their manufacturing methods, especially the chemical ones, as well as their various potential applications in many technological devices.

II.1.2. Thin film definition

A thin layer of a given substance is the material deposited on a substrate, one of its dimensions, called thickness, is greatly reduced so that it is expressed in nanometer and becomes quasi-two-dimensional material. This affects the majority of the physical properties of thin films, for which, on the contrary for a bulk, one can not neglect the effect of the boundary surfaces of materials. It's worth noting that the thinner the layer, the stronger the two-dimensional effect **[2]**.

II.1.3. Thin film growth mechanisms

According to the observations of films evaporating **[3]**, film growth can be divided into steps: : **(i)** nucleation, where a small nuclei are formed which are statistically distributed over the substrate surface, **(ii)** growth of the nuclei and formation of larger islands, which often have the shape of small crystals (crystallites), **(iii)** coalescence of the islands (crystallites) and formation of a more or less connected network containing empty channels, **(iv)** filling of the channels **[4]**.

II.1.4. Thin film growth modes

Both experiment and theory of deposition at different stages of growth, have shown that three distinguishable modes of growth and nucleation can occur: **(i)** Volmer– Weber model, **(ii)** Frank–Van der Merwe model and **(iii)** Stranski–Krastanov **[5]**.

II.1.4.1. The Frank-Van der Merve mode

Frank–Van der Merwe growth (FM), or also known as 'layer-by-layer growth' is the preferred growth model for obtaining smooth films **[6]**, which grow epitaxially at a surface or interface of crystal. In FM two-dimensional (2D) growth mode, interaction between film atoms and substrate surface is greater than between neighbouring film atoms.

II.1.4.2. The Volmer-Weber mode

When the atoms of a depositing films are more tightly coupled to each other than to the substrate, the Volmer-Weber growth mode (VW) occurs. In this situation, three-dimensional (3D) islands nucleate and grow directly on the surface of the substrate **[7]**.

II.1.4.3. The Stranski-Krastanov mode

Stranski-Krastanov growth mode (SK growth mode) is an intermediate case between the preceding two modes (FM and VW), it is also called "the layer-plus-island growth mode". In this last mechanism, after the formed the two-dimensional layer, growth continues, forming 3D islands. **Figure II.1** shows the mechanism of these three growth modes.

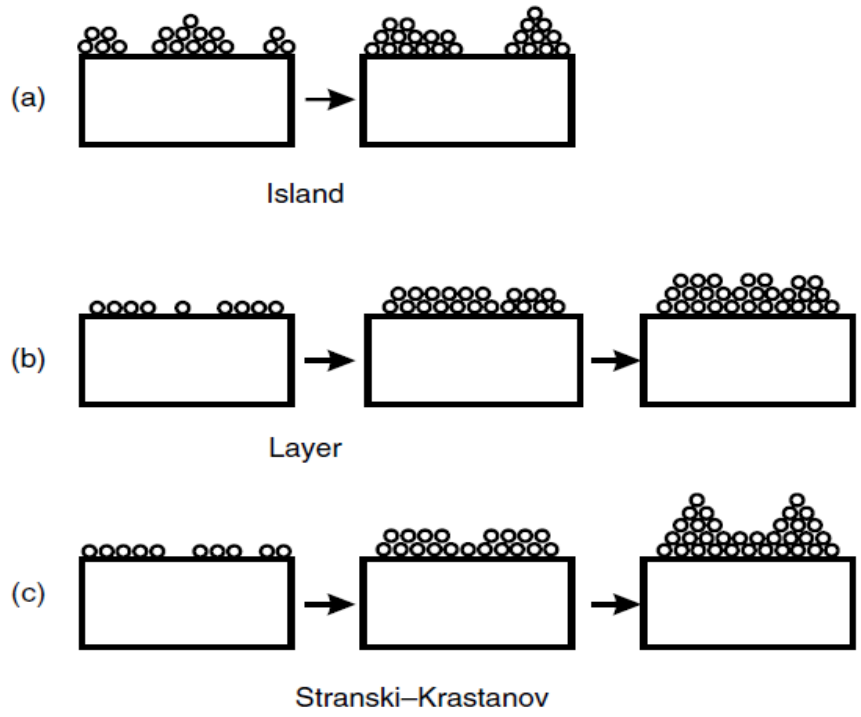

Figure II.1. Growth modes of film; **(a)** Volmer–Weber island growth **(b)** Frank–Vander Merwe layer growth and **(c)** Stranski-Krastanov layer plus island growth **[5]**.

II.1.5. Nanotechnology and nanostructured thin films

Nanotechnology is a field of innovation and development interested with the design, manufacture, and application of structures and devices by controlling their shape and size at a nanoscale as well as the fundamental understanding of the effect of material dimensions on physical properties or phenomena. Nanomaterials are of interest because they exhibit unique optical, magnetic, electrical, and other properties at such a small scale **[8]**. Nanoscale brings about giving rise to quantum phenomena that give materials new properties.

II.1.5.1. Quantum confinement

The most common effect in the nanoworld is known as quantum confinement. In this effect, the atomic structure changes due to the reduction of the nanometric scale. The quantum confinement effect produces an increase in the excitonic transition energy and a blue shift in the absorption and luminescence band gap energy as the particle size approaches the Bohr exciton radius **(Figure II.2) [9].**

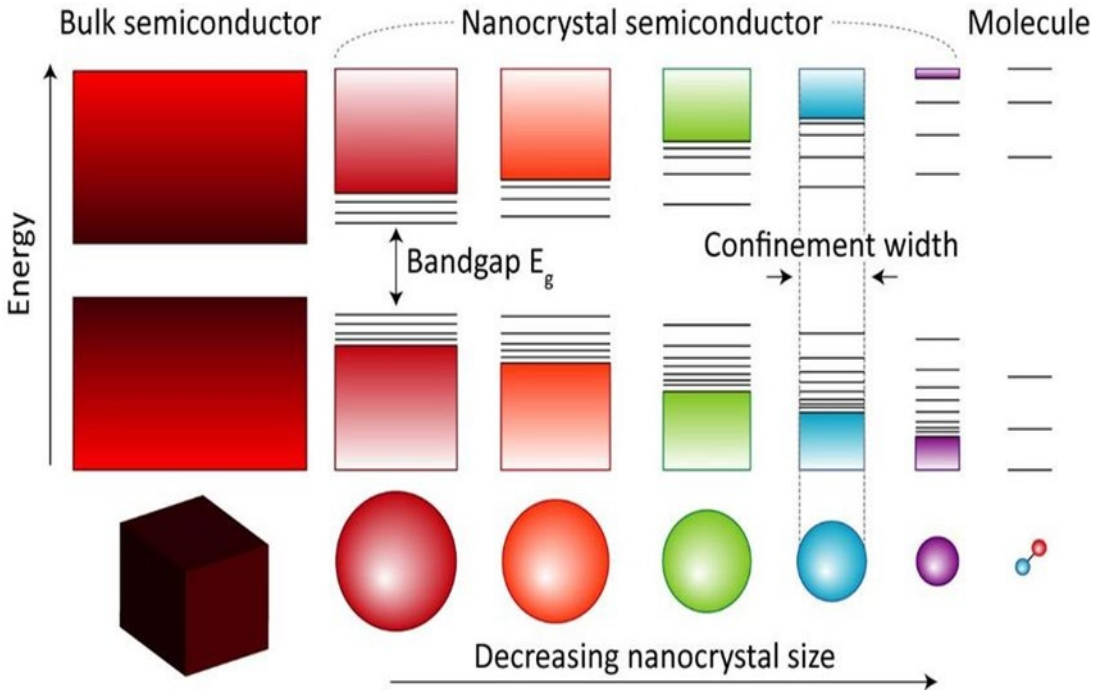

Figure II.2. Quantum confinement effect. Comparison of bulk, nanocrystals and molecules**[10] .**

II.1.5.2. Spatial confinement

Spatial confinement reflects the fact that the probability of having a defect inside a particle decreases sharply when the size becomes less than the average distance between two defects in the bulk material. In silicon, a pair of electron-hole can de-excite in two ways, either radiatively by emitting a photon of energy corresponding to the gap of the material, or non-radiatively on a crystal defect. Even for pure silicon, the second process dominates because the radius of capture of the defects is enormous (~ μm) **[2]**.

II.1.5.3. Surface effects

When the particle size significantly decreases, the surface -volume ratio increases. As an example, we refer to the materials used in applications in catalysis and detection, for which a very large specific surface area is exhibited. In the case of doped materials, increasing the surface area- volume ratio greatly increases the probability of finding the dopant on the surface. This significantly increases the efficiency of doping **[2]**.

II.1.6. General properties of zinc oxide

ZnO has three main crystalline structures, hexagonal wurtzite, cubic zincblende and rocksalt (**Figure II.3**). The wurtzite structure is the most thermodynamically stable phase. Thus, the wurtzite structure type is obtained by alternate stacking along the c direction (c-axis) of two interpenetrating hexagonal-closed-pack (HCP) sub lattices. The until cell of sub lattices forms a tetrahedron structure which consists of 5 atoms; one atom belongs to zinc (cation) and is surrounded by 4 oxygen atoms(anions) and vice versa. Moreover, the ZnO wurtzite phase has a polar hexagonal axis known as the c-axis (0002) that is parallel to the z-axis and the other is the nonpolar plane and includes $(11\bar{2}0)$ and the $(10\bar{1}0)$. The nonpolar surface has a higher surface energy compared to the polar surface. At room temperature (RT), the lattice parameters of ZnO wurtzite structure are found to be around of $a = b = 3.2496$ Å, $c = 5.2042$ Å and $\beta = 120°$, with a ratio of $c/a = 1.601$ which is close to that of an ideal compact hexagonal structure (c/a =1.633), The point group is C6v (6 mm) and the space group is P63mc in Schoenflies notation and in Hermann–Mauguin notation **[11]**.

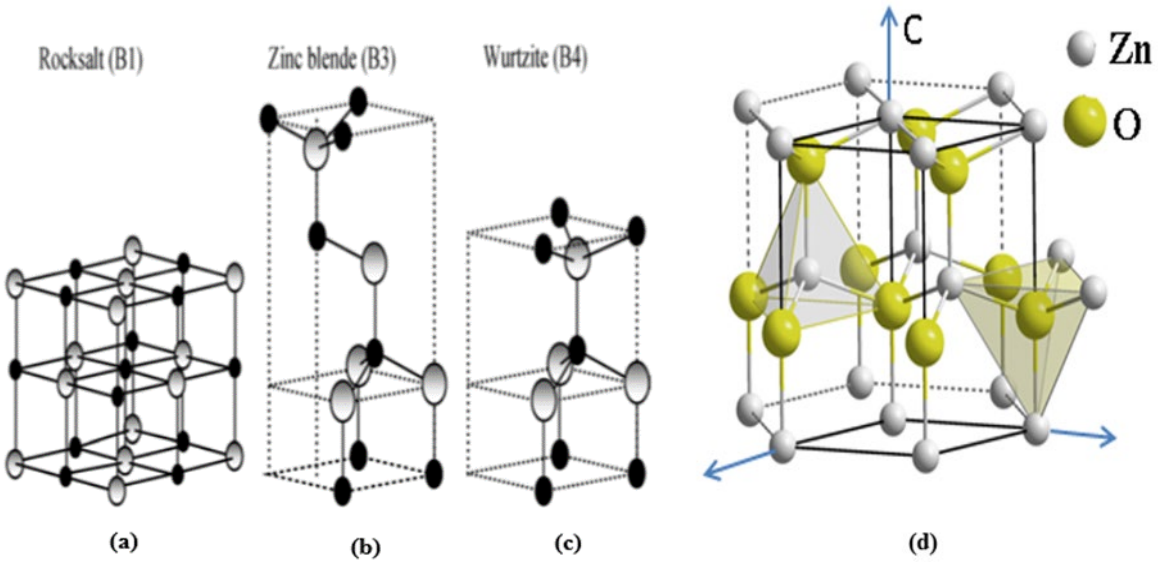

Figure II.3. Stick-and-ball representation of ZnO crystal structures: **(a)** cubic rocksalt, **(b)** cubic zinc blende, and **(c)** hexagonal wurtzite. Shaded grey and black spheres denote Zn and O atoms, respectively and **(d)** The hexagonal wurtzite structure (HCP-type) of the ZnO semiconductor **[2]**.

II.2. Sol gel technique

II.2.1 Introduction

Figure II.4 displays the schematic illustration of different routes in the sol-gel process providing various types of substances. By evaporating the liquid phase from the gel phase, xerogels are generated, while aerogels are created by solvent extraction under supercritical conditions. The films are prepared by a coating of the precursor solution on the substrates by means of dipping, spinning, or spraying. The solvent is eliminated during the deposition and subsequent drying process, resulting in densification of the films. Heat treatment is substantial to realize the target oxide composition and structural features.

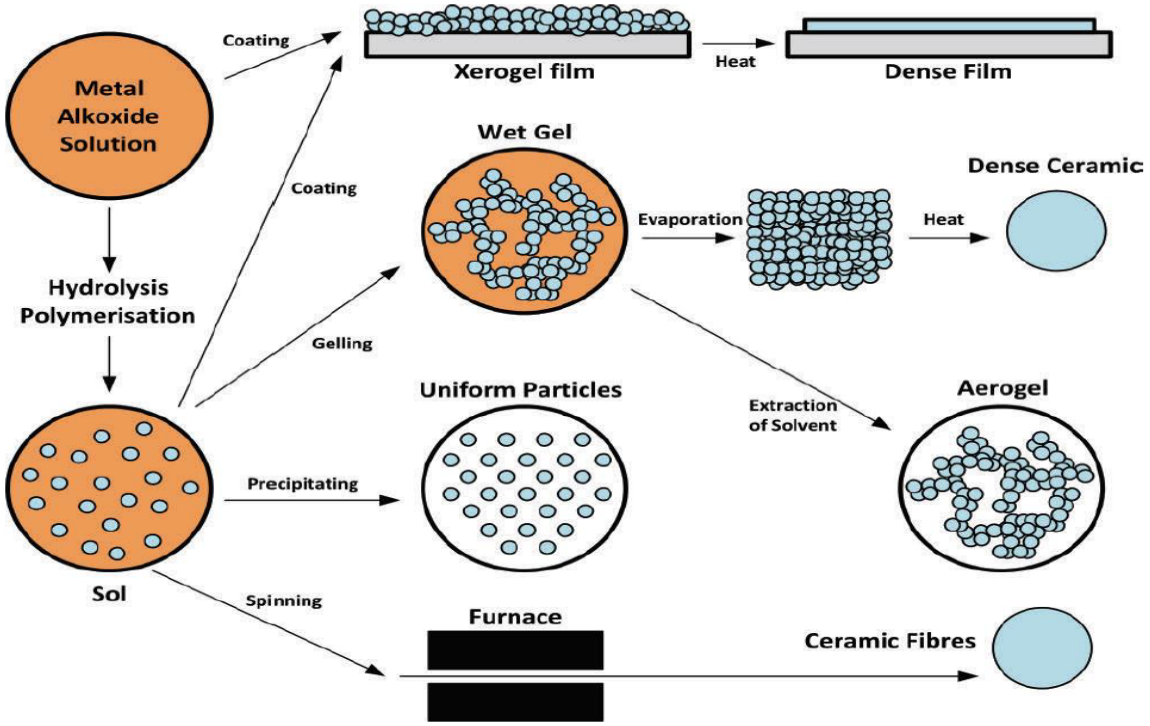

Figure II.4. Synthesis of various forms of materials by the sol-gel process **[12]**.

In the solution state, the main goal is to obtain strong homogeneity in the precursor mixture, which has significant advantages for producing a pure-phase product and can also result in lower synthesis temperatures **[13]**.The main steps of thin film preparation by the sol-gel process involve the elaboration of the precursor solution, deposition of the prepared sol on the substrate by the selected technique, and the heat treatments of the deposited films. In general, numerous parameters affect the preparation of thin films like the nature, molarty, and concentration of the chosen precursor, the choice of solvent and additives, the coating technique and deposition parameters, the nature of the substrate, and the heat treatment conditions.

Generally, the metal alkoxides of the general formulas $M(OR)_n$ are the precursors most often used in the sol-gel process, where **M** denotes a metal of valence n and R is an alkyl chain of type ($-C_nH_{2n+1}$). They can have high solubility and very high purity in a wide range of organic solvents. The synthesis, the reaction behavior, and the physical properties of the alkoxides have been extensively studied **[14,15]**, therefore, only the main characteristics necessary for understanding the reactions of alkoxides in solution will be recalled.

II.2.2. Chemical reactions

From a chemical point of view, the formation of oxide is the result of a complex succession of interconnected reactions. The basis of the synthesis is the two fundamental reactions regulating the entire sol-gel process, namely hydrolysis of the metal precursor and condensation to form the oxide network.

II.2.2.1. Hydrolysis

It is a reaction between a molecule of water and an alkoxide, allowing the releasing of a molecule of alcohol in three steps illustrated in **figure II.5**:

In order to condense the alkoxides at room temperature, the hydrolysis of the **-OR** groups must begin the reaction process. This step is necessary to give rise to the hydroxyl groups **-OH**:

- The fixing of a molecule of water on the metal atom M.
- Transfer of proton from the water molecule.
- The departure of an R-OH groups carried out by a balanced reaction process.

In a neutral condition, the reaction is written as **[16 ,17]**:

M-(OR)n+ H2O → OH-M-(OR)n-1 + R-OH

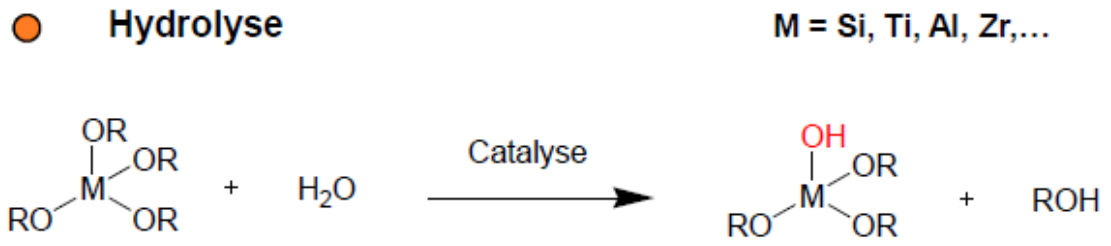

Figure II.5. Hydrolysis Mechanism of alkoxides M-$(OR)_n$ **[17]**.

This reaction can be influenced by the following parameters:

- The catalyst is acidic or basic.
- The nature of the solvent.
- The amount of water relative to the alkoxide ([H2O] / [alkoxide]).
- The temperature.

II.2.2.2. Condensation

The condensation reactions begin after the appearance of the hydroxyl groups and lead to the formation of bonds or metalloxane bridge "M-O-M". The condensation mechanism reaction may take place between the different groups. The reaction of the groups (OH-M- $(OR)_{n-1}$) gives a water molecule (the oxolation) as:

$$\mathbf{OH\text{-}M\text{-}(OR)_{n-1} + OH\text{-}M\text{-}(OR)_{n-1} \rightarrow (OR)_{n-1}\text{-}M\text{-}O\text{-}M\text{-}(OR)_{n-1} + H2O}$$

The reaction of the groups (OH-M- (OR) n-1) with remaining non-hydrolyzed groups MOR give a molecule of alcohol R-OH (the alkoxolation) as follows:

$$\mathbf{OH\text{-}M\text{-}(OR)_{n-1} + M\text{-}(OR)_{n} \rightarrow (OR)_{n-1}\text{-}M\text{-}O\text{-}M\text{-}(OR)_{n-1} + R\text{-}OH}$$

The condensation reaction mechanism is concerning to the hydrolysis reaction. Therefore, the hydrolysis parameters are also affecting the mechanism and kinetics of the reaction of condensation and, consequently, the characteristics of the obtained gel**[18]**.

II.2.3. The sol-gel transition

Growing polymer chains that agglomerate by condensation and form clusters are the most common gelation scheme. During the progression of the hydrolysis and condensation reactions, polymeric clumps, the size of which grows with time, are formed. When one of these clusters achieves an infinite size, the viscosity also becomes infinite: this is the sol-gel transition point. From this point, the infinite cluster known as the "gel fraction" expands by incorporating smaller polymeric groups. The gel is created after all of the bonds have been used **[19] .**

The evolution of a sol's viscosity and Coulomb modulus as a function of time are presented schematically in **figure II.6**. When the gel is completely formed, the viscosity becomes infinite, while the elastic constant tends to its maximum value. The solid cluster created by the base solution can then be viewed as the interleaving of polymeric chains forming a disordered solid structure. There are still trapped liquid masses in this structure. Evaporation is used to remove them**[20].**

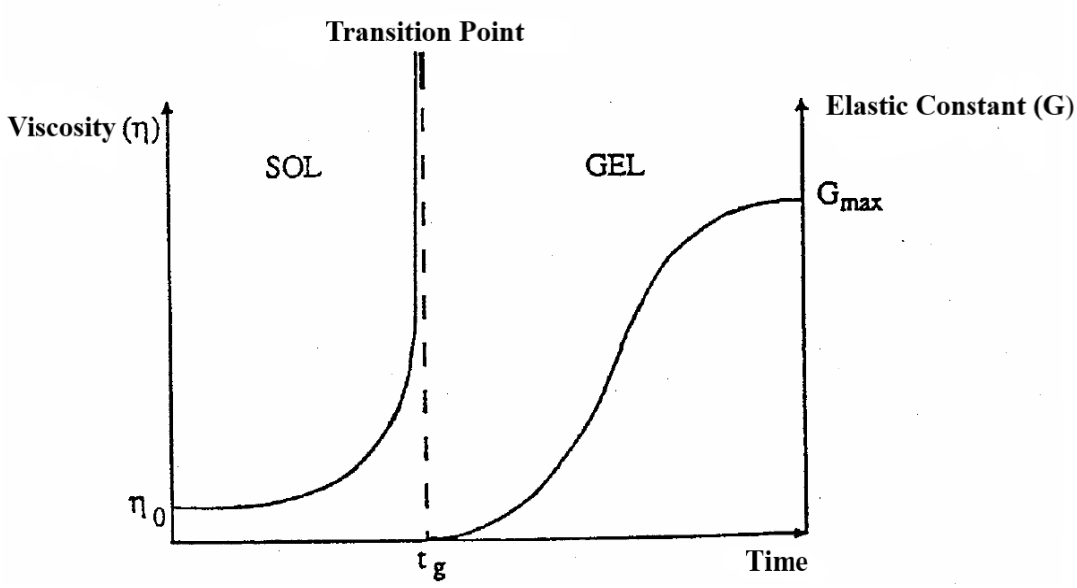

Figure II.6. Evolution of the viscosity of the solution and the elastic constant of the gel. The point **tg** corresponds to the time at the end of which the transition sol gel is reached **[19]**.

Besides, like all chemical reactions, the sol-gel transition is sensitive to its environment, such as temperature or humidity, which can thus, depending on its nature, modify the kinetics of the reactions.

II.2.4. Sol pH (Choice of catalyst)

Because of the mechanisms involved in gelation, the pH will play a significant role in the evolution of reactions. Indeed, the $\mathbf{OH^-}$ and $\mathbf{H_3O^+}$ions do not have the same influence on the reactions (hydrolysis and condensation). The $\mathbf{H_3O^+}$ cation, attracted by oxygen, facilitates the substitution of the **OR** groups and thus hydrolysis, whereas the $\mathbf{OH^-}$anion, attracted by the electronegative metal **M**, favours the formation of **M-O-M** bonds by condensation. So, a basic medium accelerates condensation, while an acidic medium promotes hydrolysis (**Figure II.7) [21, 22]**. Catalysis thus acts directly on the shape of the substance developed. This factor will also significantly influence the porosity of the final substance, hence, which partially condition the physical properties.

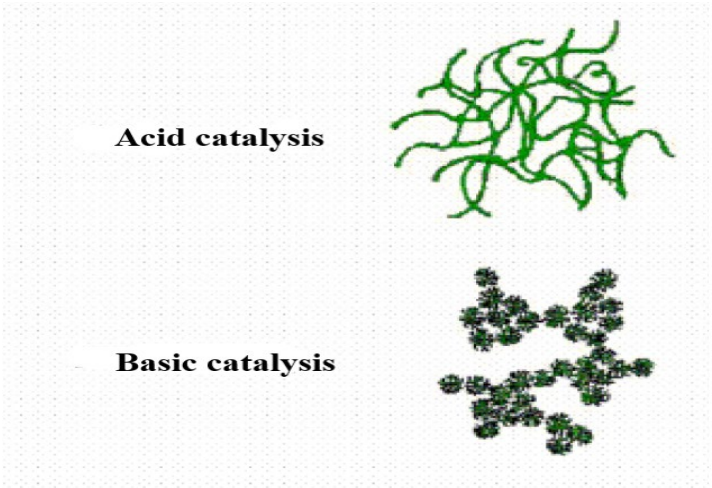

Figure II.7. Acid catalysis promotes hydrolysis and leads to the formation of longitudinal fibres. An increase in condensation generated by basic catalysis leads to clusters,characterized by a spherical shape **[23]**.

II.3. Elaboration of manganese doped zinc oxide thin films

II.3.1. Sol-gel spin-coating process

The sol-gel spin-coating technique has been usually used to synthesis manganese doped zinc oxide thin films with high purity and homogeneity. **Figure II.8** shows schematically the preparation steps of Mn doped ZnO thin films by sol-gel-spin coating method. This technique includes several steps:

- Preparation of substrates.
- Chemical preparation of the solution to acquire the liquid (Sol).
- Deposition of solution on the substrate.
- Annealed thin films to achieve in the desired crystallized and densified material.

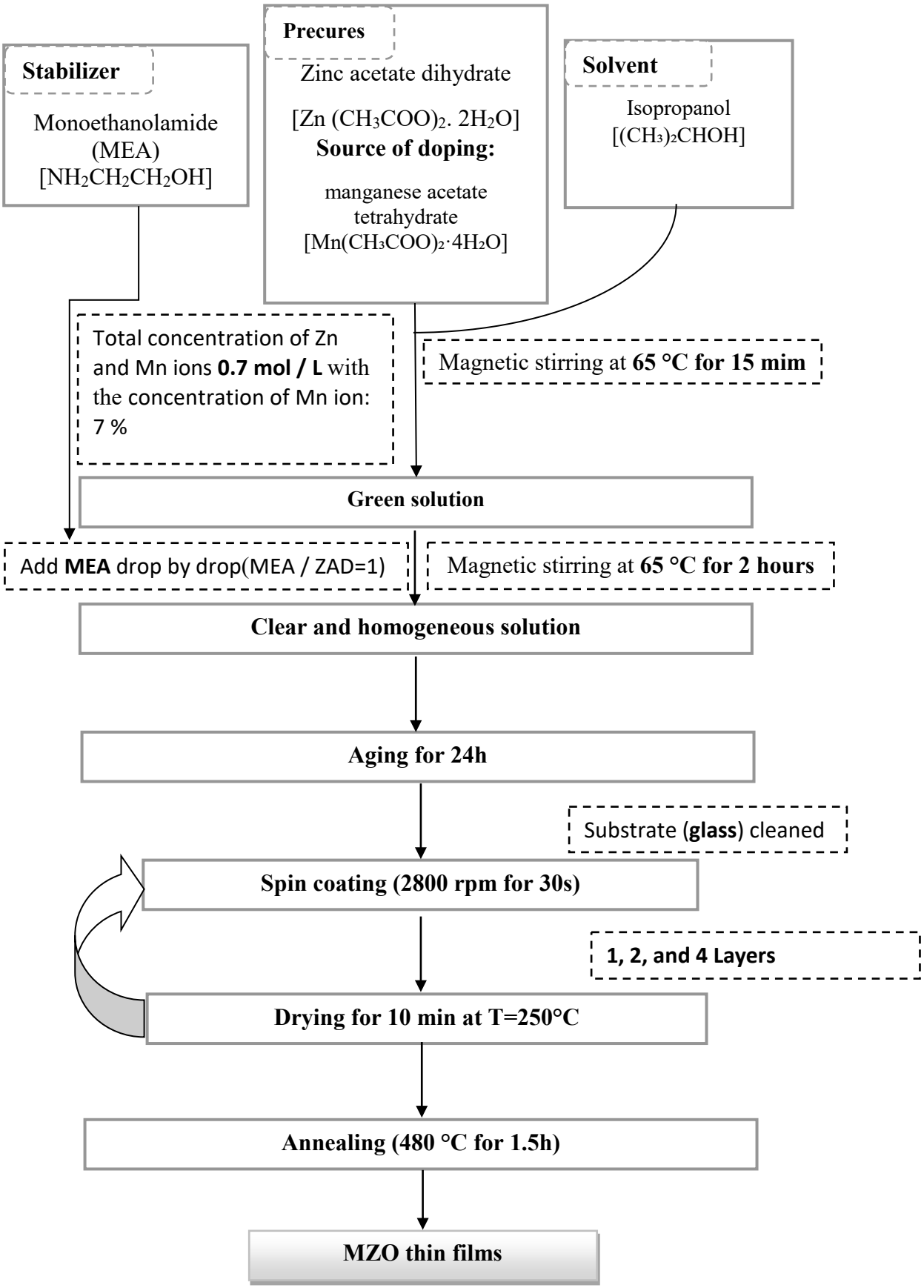

Figure II.8. Preparation steps of Mn doped ZnO (MZO) thin films by sol-gel-spin.

II.3.2. The chemical elements used in the preparation of the solution

In order to prepare starting solutions, several chemical components are used. The most important chemical and physical properties of such components are summarized in the following section:

a) Zinc acetate dihydrate: as a precursor.

Formula**: [Zn ($CH_3COO)_2$. $2H_2O$]**.

Form**:** Solid.

Color**:** White.

Melting point**:** 237 °C.

Molar mass**:** 219.49 g/mol.

Density at 20 °C**:** 1.74 g/cm^3.

Solubility in water at 20 °C**:** 430 g/l.

b) Manganese acetate tetrahydrate: as a manganese dopant source.

Formula: [$Mn(CH_3COO)_2 \cdot 4H_2O$].

Form: Solid.

Color: Pale pink.

Melting point: 80 °C (loses water of hydration).

Molar mass: 245.09 g/mol.

Density at 20 °C: ~1.59 g/cm^3.

Solubility in water at 20 °C: Soluble (approx. 72 g/L).

c) Isopropanol: Alcohol as a solvent

Formula: C_3H_8O (or $[(CH_3)_2CHOH]$)

Form: Liquid

Color: Colorless

Molar mass: 60.10 g/mol

Density: 0.786 g/cm³

Boiling point: 82.5 °C.

d) 2-Monoethanolamine -MEA: as a stabilizer or additive.
Formula**:** **$NH_2CH_2CH_2OH$.**

Form**:** Liquid.

Color**:** Colorless to yellow.

Molar mass**:** 61.08 g/mol.

Density**:** 1.01 g/cm³.

Boiling point**:** 170 °C.

II.3.3. Preparation of solutions

For the synthesis of Mn-doped ZnO solutions with varying numbers of layers (1, 2,, and 4 layers), manganese acetate tetrahydrate [$Mn(CH_3COO)_2 \cdot 4H_2O$] and zinc acetate dihydrate [$Zn(CH_3COO)_2 \cdot 2H_2O$] were used as the dopant and precursor materials, respectively. Isopropanol [$(CH_3)_2CHOH$] served as the solvent, while monoethanolamine (MEA) was used as the stabilizer. The concentration of metal ions was fixed at 0.8 M, with a MEA-to-metal ion molar ratio of 1.0. The solution was stirred at 65 °C for 2 hours and subsequently aged at room temperature for 24 hours.

To ensure the deposition of MZO thin films on clean glass substrates, these latter were cleaned in ethanol and acetone for 10 min each by using an ultrasonic cleaner and then washed with deionized water and dried.

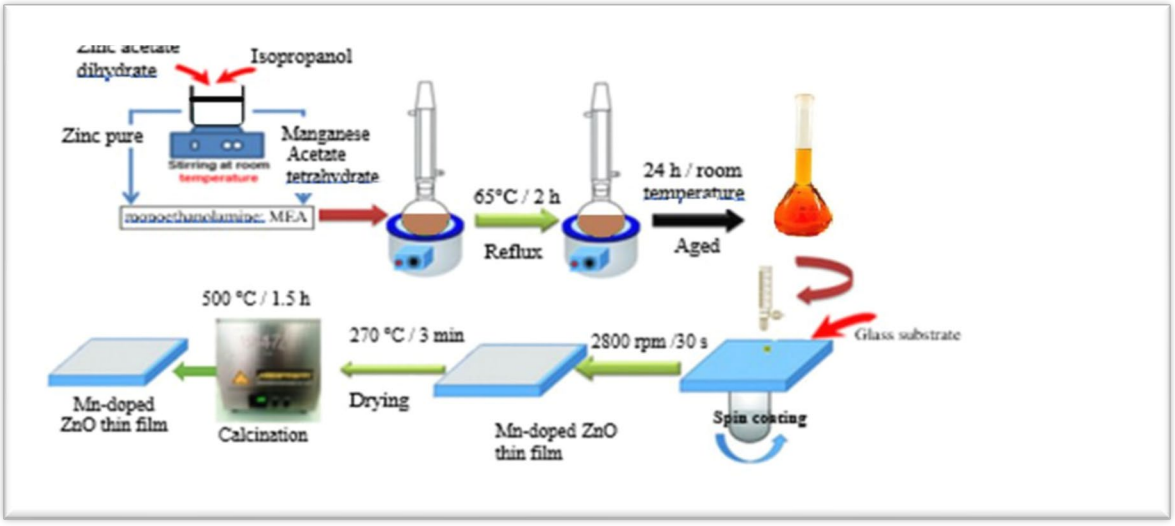

Figure II.9. Illustrative diagram of the preparation process of Mn-doped ZnO thin films.

II.4. Conclusion

This This chapter presented the various modes of thin film growth, provided a general overview of the sol-gel process, and described the experimental spin coating technique used for thin film preparation. Additionally, it It also detailed the fabrication protocol for Mn-doped ZnO thin films with a limited number of layers in order to achieve low overall film thickness.

References

[1] H. S. Nalwa, Nanostructured materials and nanotechnology: concise edition. Elsevier, 2001.

[2] A. Mahroug, “Etude des couches minces d’Oxyde de Zinc dopé Aluminium et Cobalt élaborées par la technique sol gel-spin coating.,” 2015.

[3] L. Znaidi, “Sol–gel-deposited ZnO thin films: A review,” Mater. Sci. Eng. B, vol. 174, no. 1–3, pp. 18–30, 2010.

[4] S. Abdullahi, “RF Sputtered Zinc Oxide (ZnO) Thin Films: A Review,” 2019.

[5] K. S. Harsha, Principles of vapor deposition of thin films. Elsevier, 2005.

[6] E. Alfonso, J. Olaya, and G. Cubillos, “Thin film growth through sputtering technique and its applications,” Cryst. Technol., vol. 23, pp. 11–12, 2012.

[7] C. I. Fornari, G. Fornari, H. de O. Paulo, E. Abramof, and J. dos S. Travelho, “Monte Carlo Simulation of Epitaxial Growth,” Epitaxy, p. 113, 2018.

[8] A. Sarkar, S. Roy, C. K. Ghosh, and C. K. Sarkar, “Nanoscience with Graphene,” in Nanotechnology, CRC Press, 2017, pp. 241–258.

[9] V. Arivazhagan, “Investgation of Quantum Confinement Effect in pbse znse multiple Quantum Well Structures Prepared by Thermal Evaporation technique,” 2013.

[10] J. McKittrick and L. E. Shea-Rohwer, “down conversion materials for solid-state lighting,” J. Am. Ceram. Soc., vol. 97, no. 5, pp. 1327–1352, 2014.

[11] C. Jagadish and S. J. Pearton, Zinc oxide bulk, thin films and nanostructures: processing, properties, and applications. Elsevier, 2011.

[12] C. J. Brinker and G. W. Scherer, Sol-gel science: the physics and chemistry of sol-gel processing. Academic press, 2013.

[13] A. E. Danks, S. R. Hall, and Z. Schnepp, “The evolution of ‘sol–gel’chemistry as a technique for materials synthesis,” Mater. Horizons, vol. 3, no. 2, pp. 91–112, 2016.

[14] G. E. Coates, “Metal Alkoxides: by DC Bradley, RC Mehrotra and DP Gaur, Academic Press, London, New York, San Francisco, 1978, viii+ 411 pages, $58,£ 28.” Elsevier, 1979.

[15] R. C. Mehrotra, “Synthesis and reactions of metal alkoxides,” J. Non. Cryst. Solids, vol. 100, no. 1–3, pp. 1–15, 1988.

[16] F. Collignon, “Cahier technologique sol-gel,” Ed. par Certech, pp. 0–140, 2008.

[17] T. Schneller, R. Waser, M. Kosec, and D. Payne, Chemical solution deposition of functional oxide thin films. Springer, 2013.

[18] A. Noua and R. Guemini, “Preparation and characterization of thin films nanostructures based on ZnO and other oxides,” 2019.

[19] S. Rabaste, “Microcavités optiques élaborées par voie sol-gel: applications aux ions terre rare d’Eu3+ et aux nanocristaux semiconducteurs de CdSe.” Université Claude Bernard-Lyon I, 2003.

[20] T. Gacoin, L. Malier, and J.-P. Boilot, “Sol–gel transition in CdS colloids,” J. Mater. Chem., vol. 7, no. 6, pp. 859–860, 1997.

[21] D. Gallagher and T. Ring, “Sol--Gel Processing of Ceramic Films,” Chimia (Aarau)., vol. 43, no. 10, pp. 298–304, 1989.

[22] E. J. A. Pope and J. D. J. Machenzie, “Non-cryst,” Solids, vol. 101, pp. 198–212, 1988.

[23] A. Certch, “Cahier technologique Sol-Gel,” Cent. ressources Technol. en Chim.

CHAPTER III

Results and discussions

III.1. Introduction

Several experimental studies have been conducted on Mn-doped ZnO. However, most of these studies focus on Mn-doping of ZnO thin films with relatively high thickness. The present study is dedicated to the fabrication of manganese-doped zinc oxide (MZO) thin films with a limited number of layers (x), where x = 1, 2 and 4 layers. The structural, morphological, and optical properties of MZO thin films are then characterized using various techniques, which were to be the subject of the present work.

III.2. Characterization techniques

Various techniques were employed to investigate the fabricated MZO thin films. X-ray diffractometer XRD (Broker advance Solution D8 X-ray diffractometer with Cu-kα radiation λ=1.5406 Å) was used to derive XRD diffractograms from which the Strain, crystallite size, texture coefficient, and lattice parameters are deduced. The surface morphology was studied with Field emission scanning electron microscopy FESEM (Carl Zeiss Aurga) and Atomic Force Microscopy AFM (NanoNavi /SPA 400). These techniques were used to analyze the grain size, elemental analysis, and roughness. Ultraviolet-visible UV-Vis spectrophotometer (VARIAN Carry 50) was used to investigate the transmission and reflectance spectra, from which the absorption coefficient, complex refractive index, dielectric function, and bandgap were then deduced.

III.3. Structural properties

The structural properties of Mn-doped ZnO thin films were studied by XRD .The three main peaks (100), (002), and (101) in the XRD patterns were observed **(Figure III.1)**. These peaks indicated that the Mn-doped ZnO thin films are polycrystalline and hexagonal wurtzite structure with a preferential orientation along the c-axis. Also, any secondary phase was detected in the Mn-doped ZnO films, such as $ZnMnO_3$ or Mn_3O_4**[1-3]**. It also showed there were no significant changes in the wurtzite structure after the substitutional incorporation of Mn^{+2} into ZnO host**[4]**. However, the (002) diffraction peak was observed stronger compared to the other peaks indicating that the common direction along the c-axis was the preferential growth direction. This indicated that the surface free energy of (002) planes was the most stable compared to others.

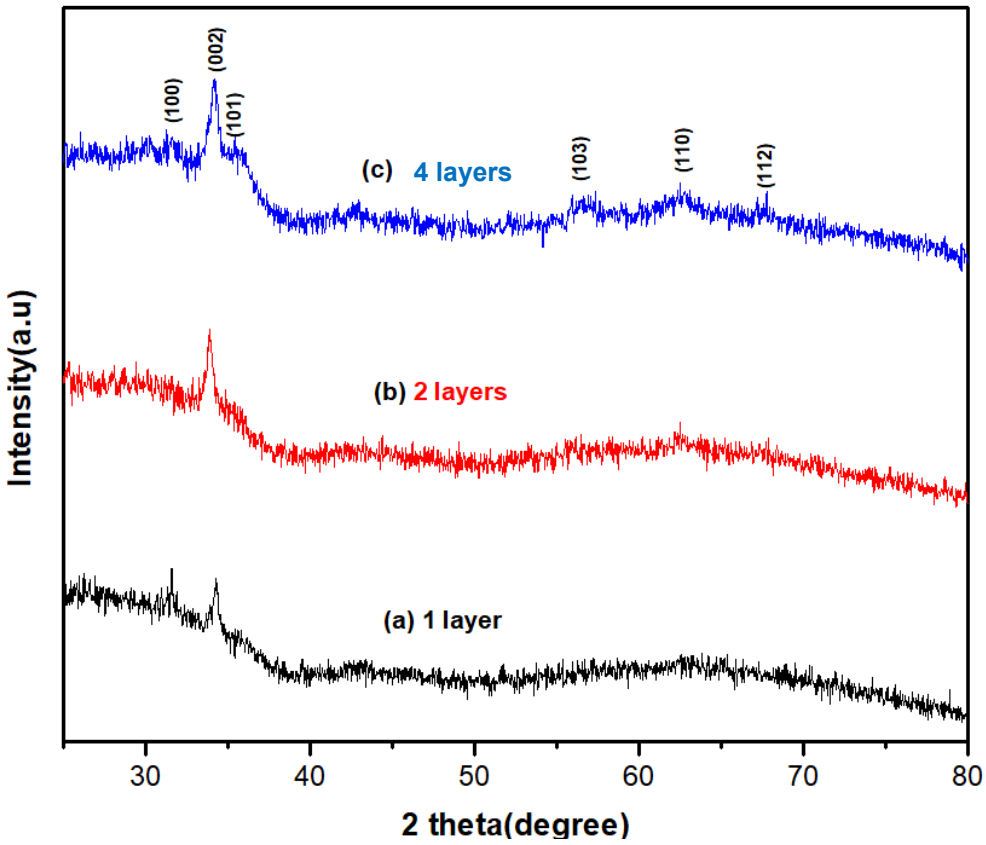

Figure III.1. XRD patterns of Mn-doped ZnO thin films for various deposited layer.

III.3.1 Lattice parameters

In the case of a hexagonal structure, such as ZnO wurtzite structure, we are interested in two parameters a=b and c. The analytical method used to calculate these parameters, is governed by the following formula:

$$sin^2\theta = {\lambda^2}/{4}\left[{4}/{3}\,(h^2 + hk + k^2)/a^2 + {l^2}/{c^2}\right] \qquad \textbf{(III.1)}$$

where θ is the diffraction angle, λ is the wavelength of the incident Cu-Kα radiation (λ =0.15406 nm) and h, k, l is the Miller indices.

From this formula, we can determine the lattice parameters a=b and c by taking into account the positions of their corresponding peaks (100) and (002), respectively. Then, we find:

$$a = \lambda / \sqrt{3}\, sin\theta_{100} \quad \textbf{(III.2)}$$

and

$$c = \lambda / sin\theta_{002} \quad \textbf{(III.3)}$$

Table III.1 shows the lattice constants $a = b$ and c and their corresponding diffraction angle (2θ), full width at half maximum (FWHM) and peak intensity for pure and MZO thin films are calculated using XRD patterns**.** The c-axis constant of Mn doped ZnO thin films decreased slightly from 5.220 Å (1 layers) to 5.225 Å (4 layers) after the increase of coating number , and all obtained values were less than the bulk value 5.207 Å (JCPDS 36–1451). This variation showed inversely proportional to the slight shift toward the higher angles of the (002) peak 2θ position with the increase of the coating number**[5]**.

III.3.2 Crystallite size and Strain

The average crystallite size (D) was estimated using the Scherrer formula:

$$D = K\lambda/\beta\cos\theta \quad \textbf{(III.4)}$$

where K is the shape factor (K =0.9), λ is the X-ray wavelength (λ=1.5406Å), β is the full width at half maxima of a given diffraction peak and θ is the Bragg angle **[6]**.

The lattice strain ε is estimated using the formula:

$$\varepsilon = \beta\cos\theta/4 \quad \textbf{(III.5)}$$

where β is the full width at half maximum of the corresponding peak and θ is the Bragg angle **[6]**.

Figure III.2 exhibits the crystallite size and strain values of MZO thin films with various thicknesses. The average crystallite size was calculated by Scherrer's formula using the width (FWHM) of the peak (002) for Mn-doped ZnO films with various thicknesses **(Table III.1)**. It can be seen that the crystallite size values decreased from 28.47 nm (one layers) to 14.85 Å (4 layers) with the increase of film thickness. The compressive strain increased with the increase of film thickness where the films are relaxed and become thicker **(Table III.1)**.

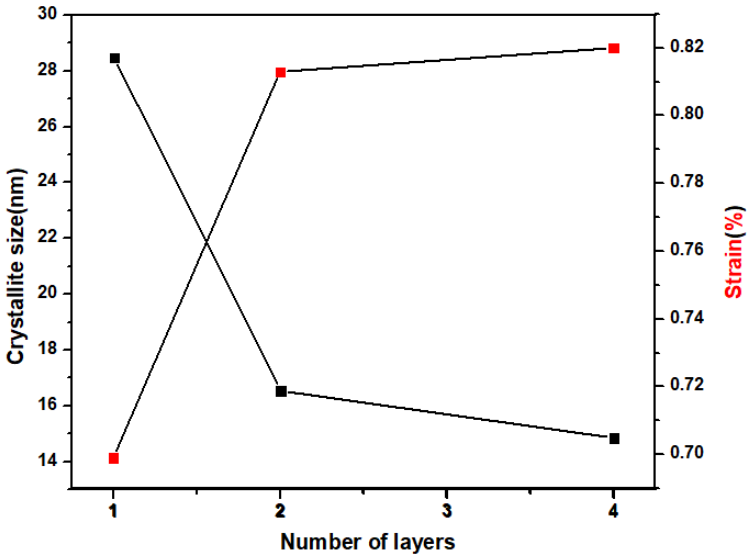

Figure III.2. Crystallite size value of MZO thin films for various deposited layer.

III.3.3 Preferred orientation

To investigate the texture of a given plane, the texture coefficient ($TC_{(hkl)}$) is needed. It measures the relative degree of preferred orientation of a plane (*hkl*). This coefficient is estimated by using:

$$TC_{(hkl)} = I_{(hkl)}/I_{0_{(hkl)}}/\left(\sum_1^N I_{(hkl)}/I_{0_{(hkl)}}\right)(1/N) \qquad \textbf{(III.6)}$$

where $I(hkl)$ and $I_0(hkl)$ are the measured relative intensity of a diffraction peak and the intensity of the standard powder diffraction peak taken from the JCPDS data, respectively, and *N* is the number of diffraction peaks **[7]**. The higher values of *TC* (greater than unity) for a given (*hkl*) direction indicate the abundance of crystallites in this direction.

TC $_{(hkl)}$ for all peaks observed in XRD patterns of Mn-doped ZnO thin films were calculated for various thicknesses **(Figure III.3)**. The highest TC (hkl) value obtained was (002) plane for all Mn doped ZnO thin films. This indicated that all films presented a preferred growth orientation along c-axis, which is (002) plane regardless of the number of deposited layers. The intensity of (002) diffraction peak increased as the film thickness increased from one layer to 4 layers. Also, the intensities of (100) and (101) peaks were found to increase with coating numbers for all Mn doped ZnO films. However, the TC (hkl) values of (101) peak were varied inversely to the (002) TC (hkl) values with the increase of thickness**[5]**.

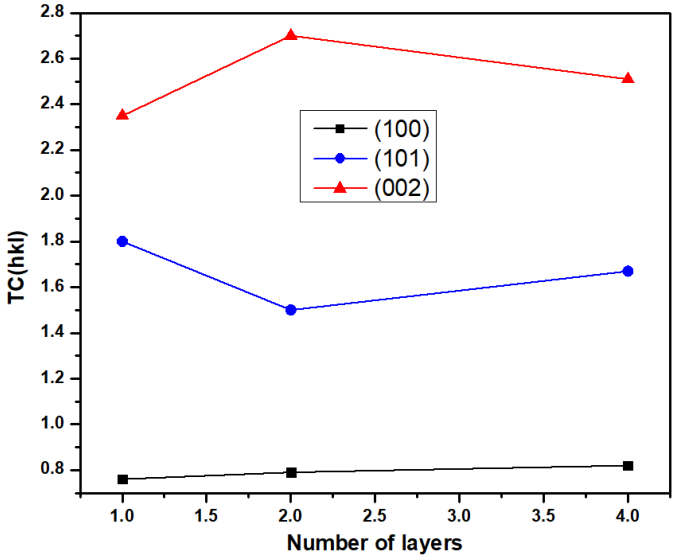

Figure III.3. Texture coefficient variation of MZO thin films for various deposited layer.

Table III.1. Morphological and structural parameters of MZO samples for various coating numbers.

Coating number	Thicknes [nm]	2θ (°)	c (Å)	FWHM (°)	Peak intensity	Crystallite size (nm)	Strain (%)
1	99	34.178	5.220	0.292	(002)	28.47	-0.699
2	291	34.238	5.225	0.502	(002)	16.54	-0.813
4	577	34.187	5.225	0.559	(002)	14.85	-0.820

III.4. Surface morphology

It is well known that microstructure is important in many applications because the properties of the materials are closely related to their crystal size, morphology, and orientation **[8]**. In this section, the surface morphology of and MZO thin films were determined by Field emission scanning electron microscopy (FESEM) and Atomic force microscopy (AFM). The crystal size, root mean squared roughness, and the growth mode are then deduced.

III.4.1 Analysis by field emission scanning electron microscopy

Figures 4. a, b,and c, display the field emission scanning electron microscopy (FESEM) 2D images and corresponding cross-sectional images of MZO thin films with 7% Mn content for 1, 2, and 4 layers, respectively. All FESEM images were captured at a magnification of 20,000×. The images reveal a morphology characterized by irregularly sized aggregated clusters. The film thicknesses, estimated from the cross-sectional images, ranged from approximately 99 to 577 nm

(inset in Figure III.4), varying with the number of deposition layers: 99 nm for 1 layer, 291 nm for 2 layers, and 577 nm for 4 layers.

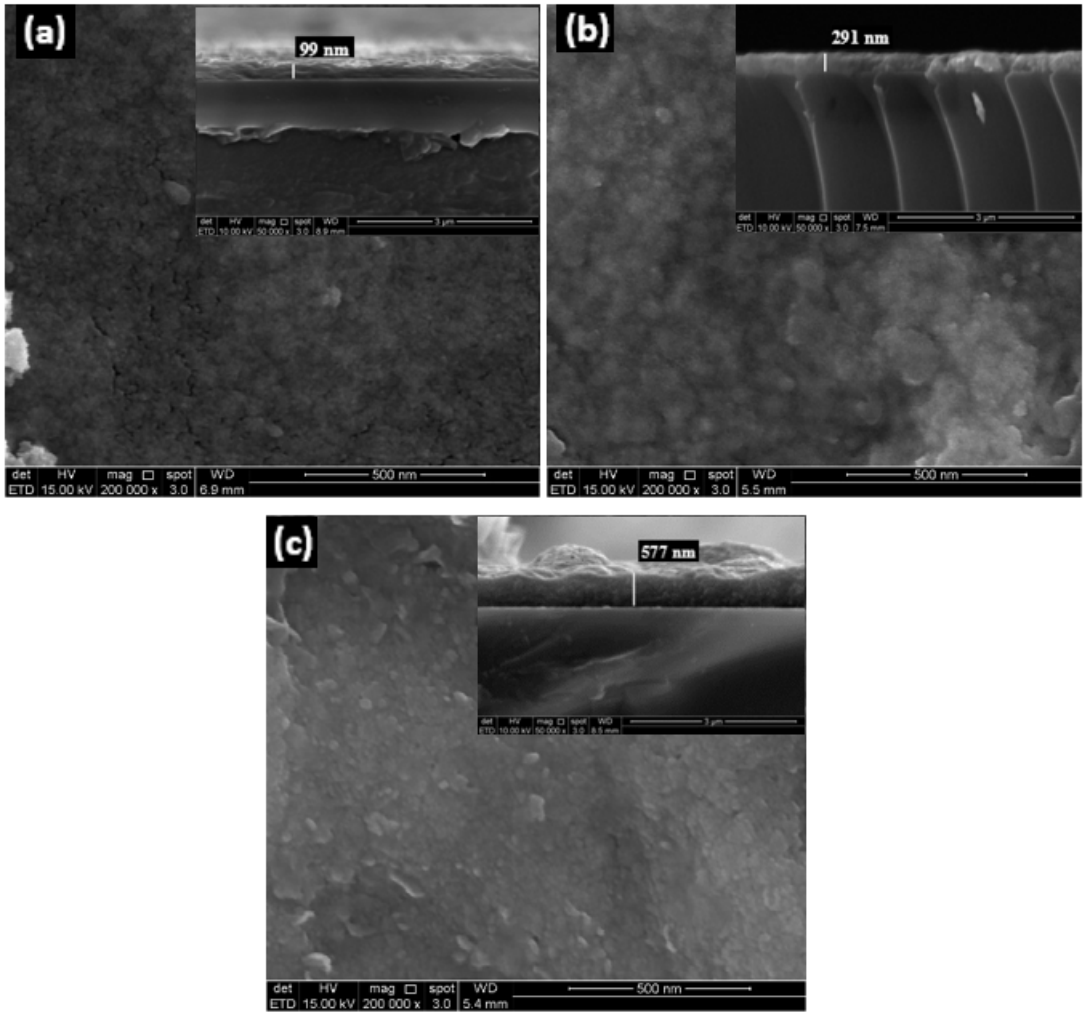

Figure III.4. FESEM 2D images and the cross-sectional images of MZO samples: **(a)** 1 coating, **(b)** 2 coatings, **(c)** 4 coatings.

III.4.2 Analysis by atomic force microscopy

Naturally, the film thickness was found to increase with coating number. The average thickness obtained from each layer was about 39 nm (Table 2). The morphology properties of Mndoped ZnO thin films with various thicknesses were investigated by AFM analysis. The 3D AFM images scanned over an area of 1.0 × 1.0 μm2 (Figure 3). The grain size and the surface roughness were extracted from the AFM images (Table 1) using WsXM software **[9]**.

Figures III.5 a, b, and c show the 1.0 X 1.0 μm^2 two and their corresponding three-dimensional AFM images for MZO thin films of MZO thin films with 7% Mn content for 1, 2, and 4 layers, respectively.The AFM images showed clearly that the samples presented a uniformly round shaped grains in a plane for all samples. The size of their grains generally increased by increasing the coating number. This result means that the growth of grains mainly vertical along (002) direction perpendicular to the substrate surface. This result is in agreement with our XRD analysis. The surface roughness of the films found to slightly increased with the thickness**[5, 10]**.

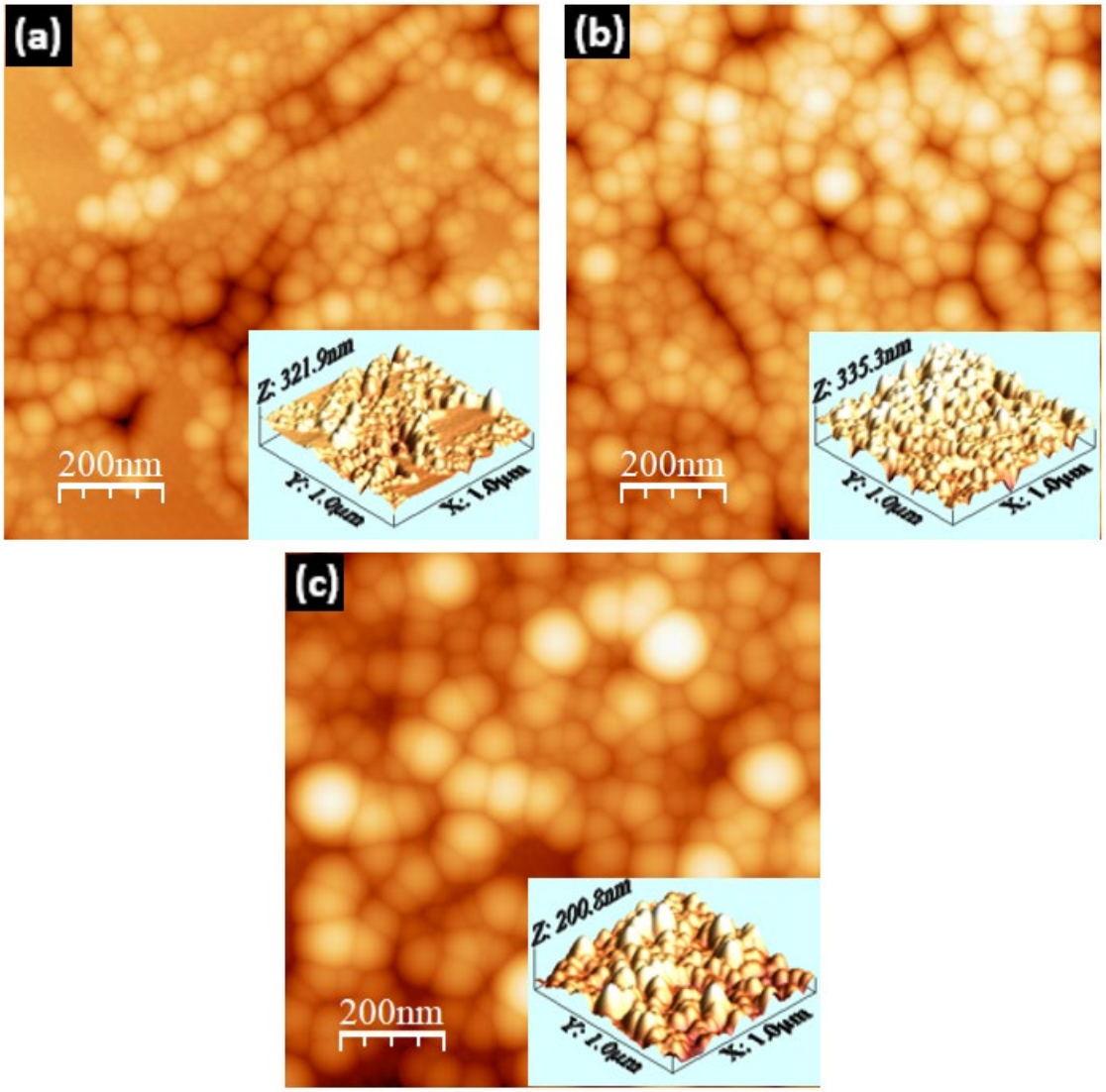

Figure III.5. 1.0 X 1.0 μm^2 Two and three-dimensional AFM images of MZO thin films ; a)1 layer, b) 2 layers, c) 4 layers.

Table III.2. Thickness, Grain size and root mean squared roughness of MZO thin films for various deposited layer

Coating number	Thickness [nm]	Grain size (AFM) (nm)	*Rrms* (nm)
1	99	26.45	20.40
2	291	24.66	20.26
4	577	42.23	33.60

III.5 Optical properties

III.5.1 Transmittance and reflectance spectra

The optical properties of Mn-doped ZnO thin films for film thickness variation were investigated (**Figure III.6**). The UV-visible was performed in the wavelength range of 350–800 nm at room temperature. In the visible range, the transmittance generally decreased with the increase of coating number of Mn-doped ZnO thin films (**Figure III.6**). A broadening of the absorption edge was observed in all Mn-doped thin films as the thickness increased, accompanied by a noticeable red shift. The highest average transmittance was recorded in the film with the lowest thickness (one-layer sample), reaching slightly below 65%. It is well known that increasing film thickness enhances light scattering, which in turn reduces the transmittance**[5]**.

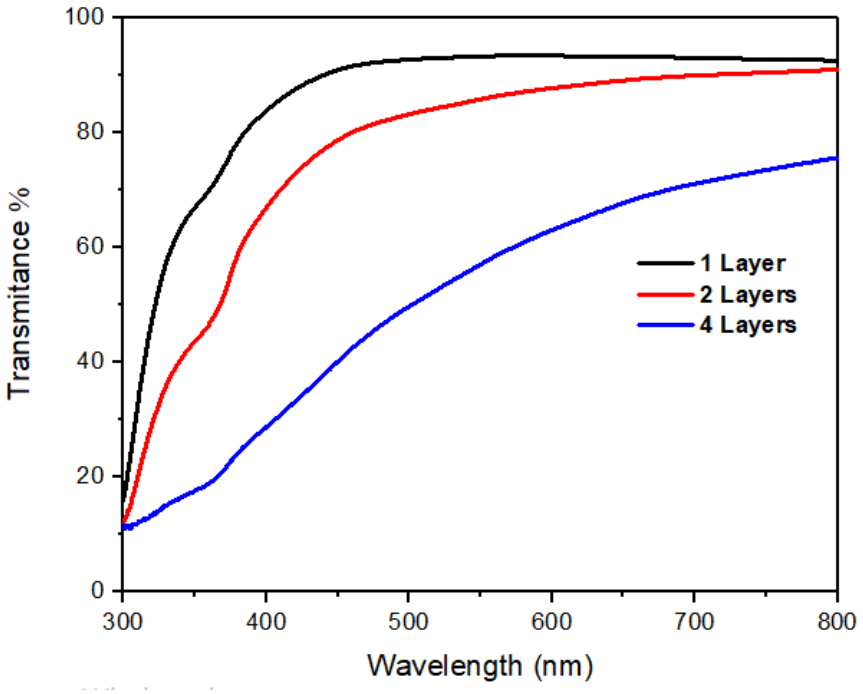

Figure III.6. Transmittance spectra of 4% Mn-doped ZnO thin films for various deposited layers.

III.5.2 Optical band gap

The transmission spectra of pure and MZO thin films in the wavelength range 350–1000 nm **(Figure III.6)**, were also exploited to deduce the band gap *Eg* using the Tauc's equation **[11, 12]**:

$$\alpha h\nu = C(h\nu - Eg)^n \qquad \textbf{(III.7)}$$

where n assumes the values 1/2, 2, 3/2 and 3 for the allowed direct, the allowed indirect, forbidden direct and forbidden indirect transitions, respectively, α is the absorption coefficient, C is a constant related to the extent of the band tailing, $h\nu$ is the photon energy and Eg is the optical band gap of the semiconductor.

The sharp absorption edge observed in the UV region (350–400 nm) for all films shifts toward longer wavelengths as the number of coating layers increases. This red shift is accompanied by a noticeable decrease in the optical band gap values, from 3.15 eV to 2.03 eV, as the number of layers increases from one to four (as shown in the **inset of Figure III.7**). This variation is attributed to changes in strain along the c-axis. These optical characteristics, combined with the ability to tune the film's properties by adjusting the number of layers, highlight the potential of Mn-doped ZnO thin films for solar cell applications, where effective UV absorption and broader light spectrum utilization are essential for improving energy conversion efficiency.

.

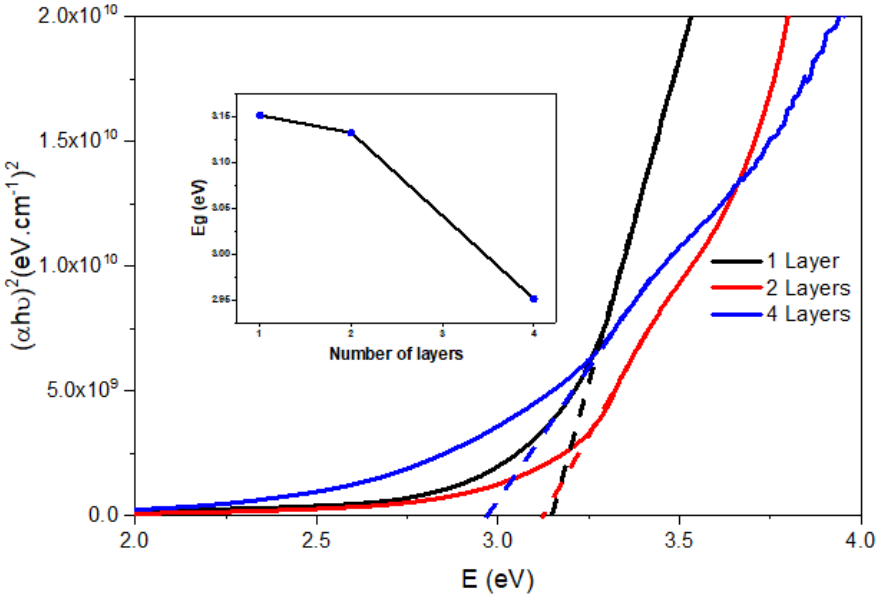

Figure III.7. $(\alpha h\nu)^2$ versus photon energy hν of Mn-doped ZnO thin films for various deposited layers. Band gap variation was also shown in the inset.

III.4. Conclusions

The thickness effect on the structural, optical, electronic and morphological properties of 7% Mn-doped ZnO thin films, were investigated. The films presented polycrystalline hexagonal wurtzite structure with a preferential orientation along the (002) axis. The (002) intensity peak increased with thickness for Mn-doped ZnO films. The result showed that the crystallite size decreased with thickness, while the c parameter slightly increased. The samples presented a uniform round shaped grains in the plane. Their grain size was marked an appreciable increase with thickness, while the roughness was found to increase slightly. The band gap varied in the range of 3.15 to 2.03 eV. The result showed the highest average transmittance value was less than 65% at the lowest thickness. Therefore, the transmittance and band gap energy were found to decrease with thickness. These observations indicate that Mn doping combined with a controlled number of coatings significantly modifies the structural, morphological, and optical properties of MZO films, making them suitable for solar cell application where UV absorption and visible light transparency are desired. This study also opens perspectives for exploring other transition metal dopants to further tailor material properties for specific applications.

References:

[1] Z. N. Kayani, F. Nazir, S. Riaz, and S. Naseem, "Structural, optical and magnetic properties of manganese zinc oxide thin films prepared by sol–gel dip coating method," *Superlattices and microstructures,* vol. 82, pp. 472-482, 2015.

[2] Z. N. Kayani, B. Zulfiqar, S. Riaz, and S. Naseem, "Influence of Al percentage on the magnetic, optical, and structural properties of Al-doped CoZnO thin films," *Journal of the Australian Ceramic Society,* vol. 55, pp. 479-487, 2019.

[3] S. Fabbiyola, L. J. Kennedy, A. Dakhel, M. Bououdina, J. J. Vijaya, and T. Ratnaji, "Structural, microstructural, optical and magnetic properties of Mn-doped ZnO nanostructures," *Journal of Molecular Structure,* vol. 1109, pp. 89-96, 2016.

[4] S. Yang and Y. Zhang, "Structural, optical and magnetic properties of Mn-doped ZnO thin films prepared by sol–gel method," *Journal of magnetism and magnetic materials,* vol. 334, pp. 52-58, 2013.

[5] A. Boukhari, B. Deghfel, A. Mahroug, R. Amari, N. Selmi, and A. A. Mohamad, "Thickness Effect on the Properties of 4% Mn-Doped ZnO Thin Films Grown by Sol-Gel Spin Coating Deposition," in *Macromolecular Symposia*, 2021, vol. 397, no. 1: Wiley Online Library, p. 2000235.

[6] S. Osali, H. Esfahani, F. Dabir, and P. Tajaslan, "Structural and electro-optical properties of electrospun Cu-Doped ZnO thin films," *Solid State Sciences,* vol. 98, p. 106038, 2019, Art no. 17.

[7] R. Amari, A. Mahroug, A. Boukhari, B. Deghfel, and N. Selmi, "Structural, optical and luminescence properties of ZnO thin films prepared by sol-gel spin-coating method: effect of precursor concentration," *Chinese Physics Letters,* vol. 35, no. 1, p. 016801, 2018, Art no. 8.

[8] A. M. Peiró *et al.*, "Hybrid polymer/metal oxide solar cells based on ZnO columnar structures," vol. 16, no. 21, pp. 2088-2096, 2006.

[9] I. Horcas, R. Fernández, J. Gomez-Rodriguez, J. Colchero, J. Gómez-Herrero, and A. M. Baro, "WSXM: A software for scanning probe microscopy and a tool for nanotechnology," *Review of scientific instruments,* vol. 78, no. 1, 2007.

[10] A. Boukhari *et al.*, "Thickness effect on the properties of Mn-doped ZnO thin films synthesis by sol-gel and comparison to first-principles calculations," *Ceramics International,* vol. 47, no. 12, pp. 17276-17285, 2021.

[11] Y. Kim and J.-Y. Leem, "Effects of Precursor Concentration on Structural and Optical Properties of ZnO Thin Films Grown on Muscovite Mica Substrates by Sol–Gel Spin-Coating," *Journal of nanoscience and nanotechnology,* vol. 16, no. 5, pp. 5186-5189, 2016, Art no. 54.

[12] A. Saboor, S. M. Shah, and H. J. M. S. i. S. P. Hussain, "Band gap tuning and applications of ZnO nanorods in hybrid solar cell: Ag-doped verses Nd-doped ZnO nanorods," vol. 93, pp. 215-225, 2019.

General conclusions and perspectives

The aim of this thesis was to develop manganese-doped zinc oxide (MZO) thin films with 7% Mn content and low thicknesses (1, 2, and 4 layers) using the sol-gel method. Starting from manganese acetate tetrahydrate as the dopant source, zinc acetate dihydrate as the precursor, and isopropanol as the solvent and stabilizer, a preparation protocol was established. The Mn-doped ZnO thin films were deposited onto glass substrates using the spin coating technique.

To ensure well crystallization of the prepared thin films, ideal experimental conditions were adopted, which based on our experimental literature review, such as molar ratio of the solvent to metal ions, stirring, aging, cleaning and drying of substrates, spinning, preheating and annealing. Various techniques were employed to investigate the fabricated samples such as X-ray diffraction, Atomic Force Microscopy, Field emission scanning electron microscopy and Ultraviolet-visible UV-vis spectrophotometry.

The experimental investigations confirmed that all Mn-doped ZnO thin films exhibit a polycrystalline nature with a wurtzite hexagonal structure. Although the (002) diffraction peak remains dominant, an increased number of coating layers causes a relative enhancement of the (101) orientation. The crystallite size and lattice strain are notably affected by the film thickness, as confirmed by XRD analysis, where crystallite size decreases and compressive strain increases with the number of layers. Surface morphology, examined via FESEM and AFM, reveals that grain size varies irregularly and surface roughness tends to increase with thickness. Optically, the transmittance of the films in the visible region decreases with increasing thickness due to enhanced light scattering, while the band gap energy shows a red shift, shrinking from 3.15 eV to 2.03 eV. These observations indicate that Mn doping combined with a controlled number of coatings significantly modifies the structural, morphological, and optical properties of MZO films, making them suitable for optoelectronic applications where UV absorption and visible light transparency are desired. This

study also opens perspectives for exploring other transition metal dopants to further tailor material properties for specific applications.

In perspective, Mn-doping significantly influences the properties of MZO thin films at a low number of coating layers, which opens the door to considering the use of other elements from the transition metals group to further tailor and control their properties. This approach could potentially expand the range of their applications in various advanced technologies. Therefore, this issue remains an open field for further research.

Abstract

In this study, manganese-doped zinc oxide (MZO) thin films with a fixed Mn content of 7% and varying coating numbers (1, 2, and 4 layers) were synthesized using the sol–gel spin coating method. Manganese acetate tetrahydrate, zinc acetate dihydrate, and isopropanol were employed as the dopant source, precursor, and stabilizing solvent, respectively. XRD analysis revealed that all MZO thin films exhibited a polycrystalline structure with a wurtzite hexagonal phase. The preferred orientation along the (002) plane was observed. The crystallite size decreased while the lattice strain increased with film thickness. Surface morphology analysis using FESEM and AFM indicated irregular grain distribution and a gradual increase in surface roughness. Optical measurements showed that the transmittance of the films in the visible region decreased with increasing thickness, while the optical band gap exhibited a red shift, narrowing from 3.15 eV to 2.03 eV. These results demonstrate that Mn doping and layer control significantly affect the structural, morphological, and optical properties of ZnO thin films, making them promising candidates for solar cell application.

Key-Words: Manganese -doped zinc oxide thin films; Sol-gel technique; Eg; Spin coating method; solar cell application.

ملخص

في العمل الحالي، تم تحضير الطبقات الرقيقة ل في هذا العمل، تم تحضير الطبقات الرقيقة لأكسيد الزنك المطعّم بالمنغنيز (MZO) بنسبة تطعيم ثابتة تبلغ 7% وعدد طبقات مختلف (1، 2 و4 طبقات) باستخدام طريقة الطلاء بالتدوير بطريقة محلول–هلام .(Sol-Gel) استُخدم كل من كلوريد المنغنيز الثنائي كمصدر للتطعيم، وخلات الزنك ثنائي الهيدرات كمادة بادئة، والإيزوبروبانول كمذيب ومثبت. أظهرت نتائج حيود الأشعة السينية (XRD) أن جميع الطبقات الرقيقة المحضّرة تمتلك بنية متعددة البلورات بطور وورتزيت سداسي، مع تفضيل في النمو على طول المستوي (002). تناقص الحجم البلوري مع زيادة السماكة، في حين ازدادت الإجهادات البلورية. كشفت دراسة شكل السطح باستخدام كل من المجهر الإلكتروني الماسح الباعث للإلكترونات (FESEM) والمجهر الذري للقوة (AFM) عن توزيع غير منتظم للحبيبات وازدياد تدريجي في خشونة السطح. أما الخواص البصرية، فقد أظهرت أن النفاذية في المنطقة المرئية انخفضت مع زيادة عدد الطبقات، في حين أظهرت فجوة الطاقة البصرية (Eg) انزياحاً نحو الأطوال الموجية الأكبر(Red shift) ، متقلصة من 3.15 eV إلى 2.03 .eV توضح هذه النتائج أن تطعيم ZnO بعنصر المنغنيز والتحكم في عدد الطبقات له تأثير كبير على الخصائص البنيوية والمورفولوجية والبصرية، مما يجعل هذه الطبقات الرقيقة مرشحة واعدة لتطبيقات الأجهزة الخلايا الشمسية.

الكلمات المفاتيح: الطبقات الرقيقة لأكسيد الزنك المطعّم بالمنغنيز ؛ ؛ تقنية محلول–هلام؛ فجوة الطاقة(Eg) ؛ طريقة الطلاء بالدوران؛ التطبيقات الخلايا الشمسية.